RESPONSES TO

NRC QUESTIONS

ON THE

MONTICELLO PUAR

PREPARED BY

NUTECH ENGINEERS, INC.

SAN JOSE, CALIFORNIA

PREPARED FOR

NORTHERN STATES POWER CO.

nutech ENGINEERS

NRC QUESTION ON MONTICELLO PUAR HYDRODYNAMIC LOAD RESPONSE

ITEM 1: Acceleration volumes for the ring girder submerged structure loads (Sections 1.4.1.5, 1.4.1.6, 1.4.1.7.3, 1.4.1.8.3, 1.4.2.4 and Appendix A) are computed by an alternate method that differs from the Acceptance Criteria. The stated use of Table 1-4.1-1 is clearly not possible directly as the shapes and flow directions presented do not match any realistic model of the ring girder. The information presented in Appendix A is insufficient to determine the general conservatism of the alternate method. For segments 7, 8, 9 and 10 (Figure 2-2.2-9) give the specific procedures for calculating the acceleration volumes for loads in the directions normal to the flange, normal to the web and normal to the stiffners. For the post-chug example chosen in Appendix A identify the chugging downcomers and the phasing selected, and give the local accelerations at segments 7, 8, 9 and 10 in the x, y and z directions due to unit source strengths that were used to generate Table 2-2.2-9.

RESPONSE TO ITEM 1

The acceleration drag volume for the ring girder was initially calculated following the method described in NUREG- 0661 for structures with sharp corners, such as I-beams. That is, a cylinder is circumscribed and the volume is based on the cylinder. The SRV air bubble drag pressure calculated with the ring girder idealized as a cylinder was approximately 187 psi.(in-plane direction). However, the highest bubble pressure measured during the T-Quencher test at Monticello was 14 psi. Subsequent investigation of this discrepancy revealed that the acceleration volume based on a circumscribed cylinder was extremely conservative. An emperically derived volume was then estimated as follows.

The model that predicts torus shell pressures due to SRV actuations (QBUBS02) was used to calculate the peak pressure at the ring girder location and then this pressure (12.2 psi) was compared to the one derived from the submerged structure model (187 psi) results. The ratio of these pressures gives the value by which the ring girder acceleration volume based on an equivalent cylinder should be divided to yield realistic results. Note that this value is still conservative since QBUBS02 was calibrated to bound all test data.

When the acceleration volume for the ring girder based on the equivalent cylinder is divided by the ratio just described, the value obtained is approximately equal to that presented in Appendix A of the Monticello PUAR.

For the post-chug example chosen in Appendix A, downcomers 2 and 3 (see Figure 1-1) chug out-of-phase, and the local accelerations due to a unit source strength in the x, y and z directions used to generate Table 2-2.2-9, are:

Section No.	Acceleration $(ft/sec^2)/(ft^3/sec^2)$		
	A_x	A_y	A_z
7	0.	0.01784	-0.01424
8	-0.00039	0.00408	-0.01316
9	0.18311E-9	0.18978E-8	-0.01416
10	0.	-0.00601	-0.01561

When the acceleration volume in the out-of-plane direction for the ring girder is calculated conservatively by modeling the ring girder as a rectangle, a value of 50.46 ft^3 is obtained for Sections 7 through 10. This value is calculated as follows:

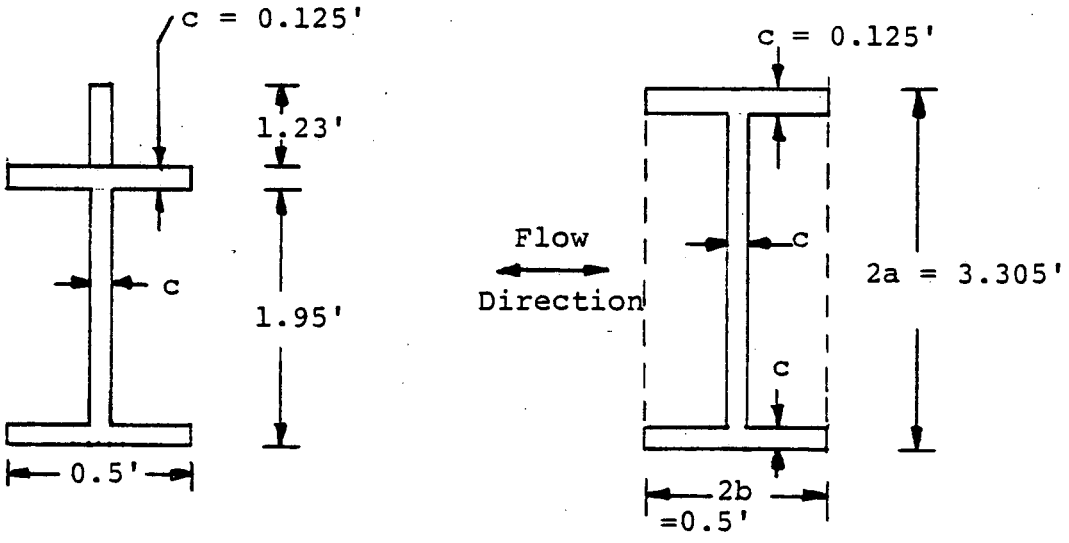

$V = \left[1.187\ \pi\ a^2 + (2a-2c) + 4cb\right]\ L A_w$ where the dimensions a, b, and c are shown above, L is the segment length (2.36') and A_w is the wall interference factor (2.0).

$V = 50.46\ ft^3$

The value of the acceleration volume presented in Appendix A of NSP PUAR is 8.50 ft^3. Thus, if the more conservative value is used, the submerged structure loads would be 5.94 (=50.46/8.50) times higher.

nutech ENGINEERS

NRC Consultants have recommended the use of the ring girder acceleration drag volume for submerged structure loads normal to the ring girder calculated above. That is, a factor of 5.94 higher than the drag volume used to develop the loads reported in the Monticello PUAR. The most highly stressed structural component that would be significantly affected by an increase in the submerged structure loads on the ring girder is the torus shell directly adjacent to the ring girder web and seismic restraint pad plate. As is shown in Table 2-2.5-9 of the PUAR, the primary + secondary stress range for this structural component is 94% of allowable for the submerged structure loads presented in the PUAR.

The effects of the increased ring girder acceleration drag volume can conservatively be evaluated by factoring up the torus shell stress components caused directly by SRV and chugging submerged structure loads acting on the ring girder. These stress components can then be absolutely summed with the other loads in the IBA III load combination. However, when the higher shell stresses due to the increasesd submerged structure loads in the ring girder are absolutely summed with the other stress components, the resultant stress intensity range exceeds the allowable by 21%.

As a reasonable alternative to absolute summation, the square root sum of the squares (SRSS) method could be used to combine the effects of statistically independent, dynamic time history loadings. The dynamic loadings that occur in the IBA III load combination are earthquake (OBE), chugging and SRV discharge. The response to each of these loadings was calculated separately. The stress components for each of the dynamic loadings are given in Table 1. Since there is no mechanistic reason why SRV discharge should have a specific time phasing, and since an earthquake is a totally random event, it is highly unlikely that peak values of response for a given structural element would

occur simultaneously. The absolute summation technique assumes that this unlikely occurrence is indeed the case. Using SRSS to combine the results of these three loadings, the calculated primary + secondary stress range is reduced to 97% of allowable even with the increased submerged structure loads on the ring girder.

LOAD CASE	σ_x (2)	σ_y (2)	τ_{xy} (2)
Static	6.10	16.45	-1.79
OBE	±.09	±3.09	± .10
Chugging Shell Pressures	±.16	±1.90	± .15
SRV Shell Pressures	+1.62	+10.96	+1.25
	-1.59	-16.30	-1.17
Chugging Ring Girder S.S. Loads (1)	± .22	± .65	± .07
SRV Ring Girder S.S. Loads (1)	±3.46	±10.85	±1.30
Vent Hdr. Support Column			
Reactions (Chugging)	±1.11	±3.44	± .41
Reactions (SRV)	± .48	±1.48	± .18
HPCI Pipe Support Reactions	± .40	±1.15	± .14
SRV Pipe Support Reactions	±1.84	±5.54	± .72

TABLE 1

MAXIMUM TORUS SHELL STRESS FOR

IBA III LOAD COMBINATIONS

Notes: (1) Stresses include effect of 5.94 factor

(2) Stresses are in ksi

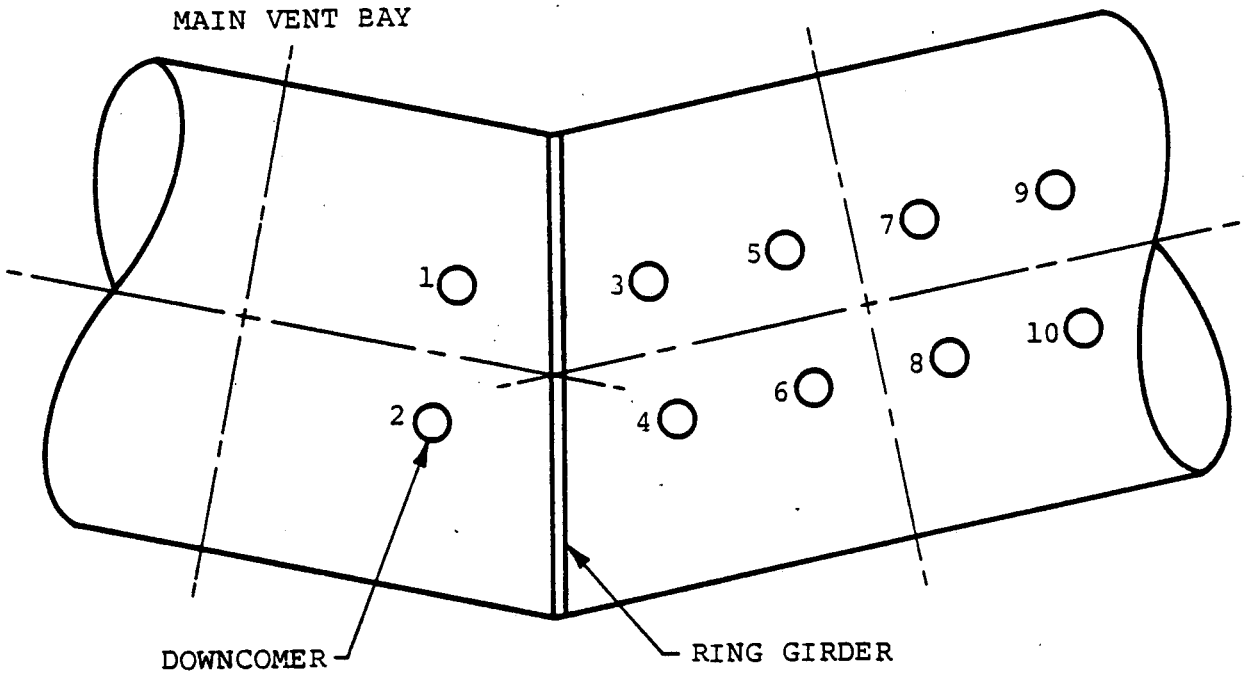

Figure 1-1

DOWNCOMER LOCATIONS

NRC QUESTION ON MONTICELLO PUAR

STRUCTURAL RESPONSE

ITEM 2: Submerged structure loads are applied by calculating an equivalent static load based on DLF's of simple single degree of freedom systems (Appendix A) with natural frequencies deduced from more elaborate structural models (Figures 2-2.4-5 and 2-2.4-9). While this may be generally conservative for beam-like structures, it is not clearly so for a more complicated structure such as the ring girder. Provide information on the ring girder mode shapes associated with the two critical frequencies (20 Hz and 25 Hz) and justify using the same DLF function of frequency for loading in all three directions on the ring girder.

RESPONSE TO ITEM 2

The methodology used in determining DLF's to be applied to the ring girder submerged structure loads was not based upon a single degree of freedom system approach. The actual approach used is as follows:

1) The suppression chamber simplified ring girder finite element model was created. (See PUAR Figure 2-2.4-5)
2) The steady state response of this structural model was determined for a sinusoidal varying unit pressure loading of the submerged web area for each 1 Hz frequency increment from 1 to 50 Hz. Structural modes up to 75 Hz were included in this response calculation. The maximum flange lateral displacement at the ring girder B.D.C. was plotted against the frequency. (See Figure 2-2.4-9).
3) The flange lateral displacement at the ring girder B.D.C. was determined for a static unit pressure loading of the submerged web area.
4) The DLF at each frequency was then calculated as the ratio of the peak displacement from Figure 2-2.4-9 to the displacement as determined in Step 3.

As can be seen from the above approach, the DLF determination was based upon a steady state dynamic analysis of the simplified ring girder model.

nutech ENGINEERS

Although this DLF was based upon the out-of-plane loading direction of the web, it is conservatively representative of the other two loading directions as well since the out-of-plane direction of the ring girder is by far the most flexible of the three principal ring girder directions and is the primary contributor to the mode shapes for frequencies below 50 Hz.

nutech
ENGINEERS

NRC QUESTION ON MONTICELLO PUAR HYDRODYNAMIC LOAD RESPONSE

ITEM 3: Submerged structure loads require a computation of the velocity and acceleration fields computed on the basis of the method of images applied to a model of the torus bay. Table 1-4.1-2 gives the relevant parameters for the rectangular bay model used for LOCA bubble drag loads. Is the same model used for CO, chugging and SRV loads on submerged structures? If yes, justify the use of this model for structures near the bay boundary (e.g. ring girder, vent header support column) under asymmetric loading conditions, i.e., sources acting in one bay only. If not, describe in detail the models used.

RESPONSE TO ITEM 3

The rectangular bay model for CO, chugging and SRV loads on submerged structures is similar to that used for LOCA bubble drag loads.

As required in Appendix A of NUREG0661, Model E in NEDE-21983-P is used for the method of images simulation of the torus cross-section for LOCA air bubble, CO, chugging and SRV analyses.

The length of the bay model for LOCA air bubble analysis is equal to one actual bay and structures may be close to the bay boundary.

However, for the CO, chugging and SRV analyses, structures are always placed at or very near the center of the rectangular bay model ($\frac{1}{2}D$) as shown in Figures 3-1, 3-2, 3-3, and 3-4. From these figures it can be seen that the torus is unwrapped to a length D which is equal to the torus circumference ($D = 2\pi R_{major}$, $D_{Monticello} \sim 308ft$). Hence, structures are never near the bay boundary and asymmetric loading conditions, i.e., sources acting in one bay only, are readily accommodated.

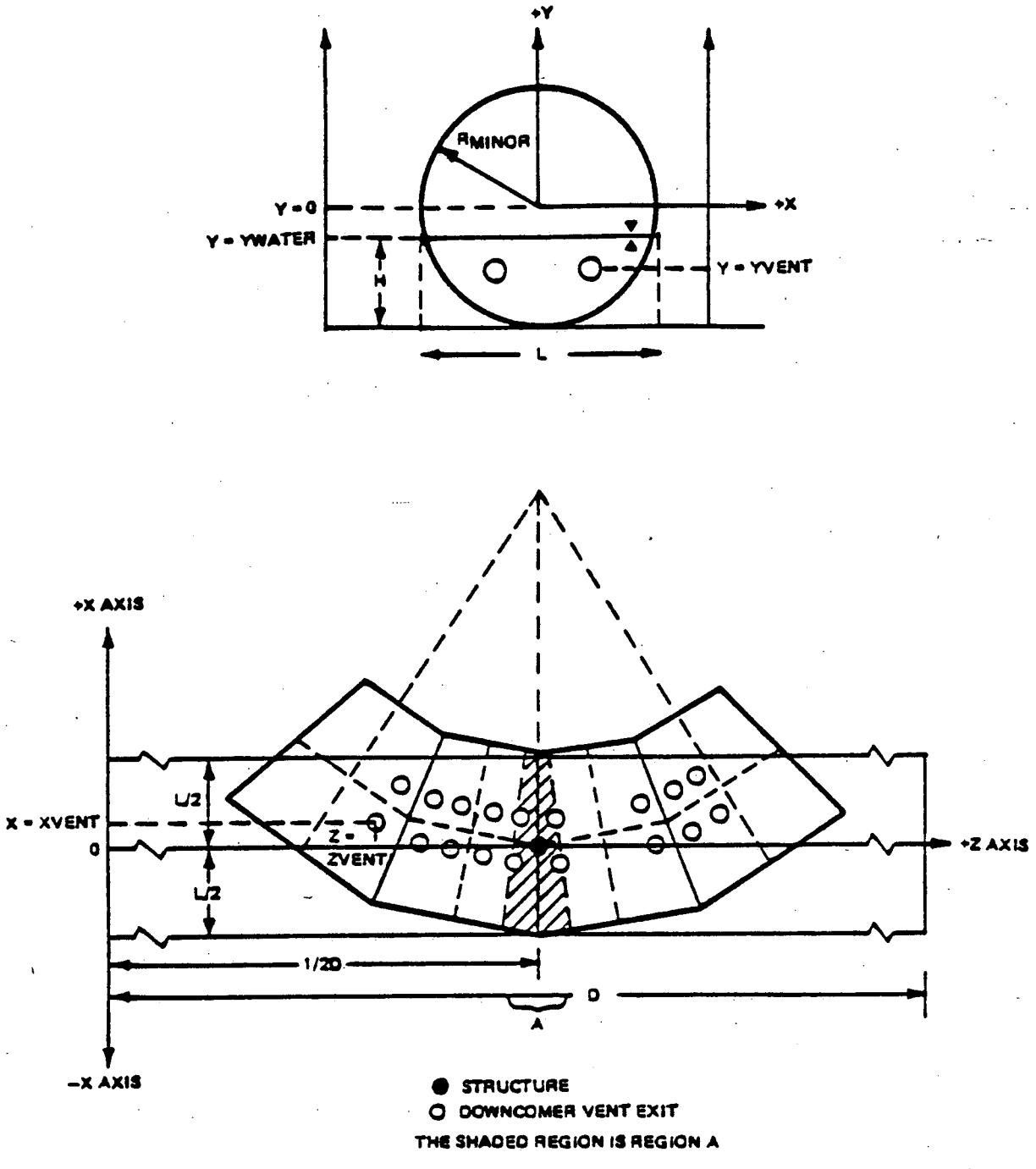

Figure 3-1

RECTANGULAR CELL MODELING FOR PLANTS WITH 96 DCS C.O. AND CHUGGING (CELL A)

nutech ENGINEERS

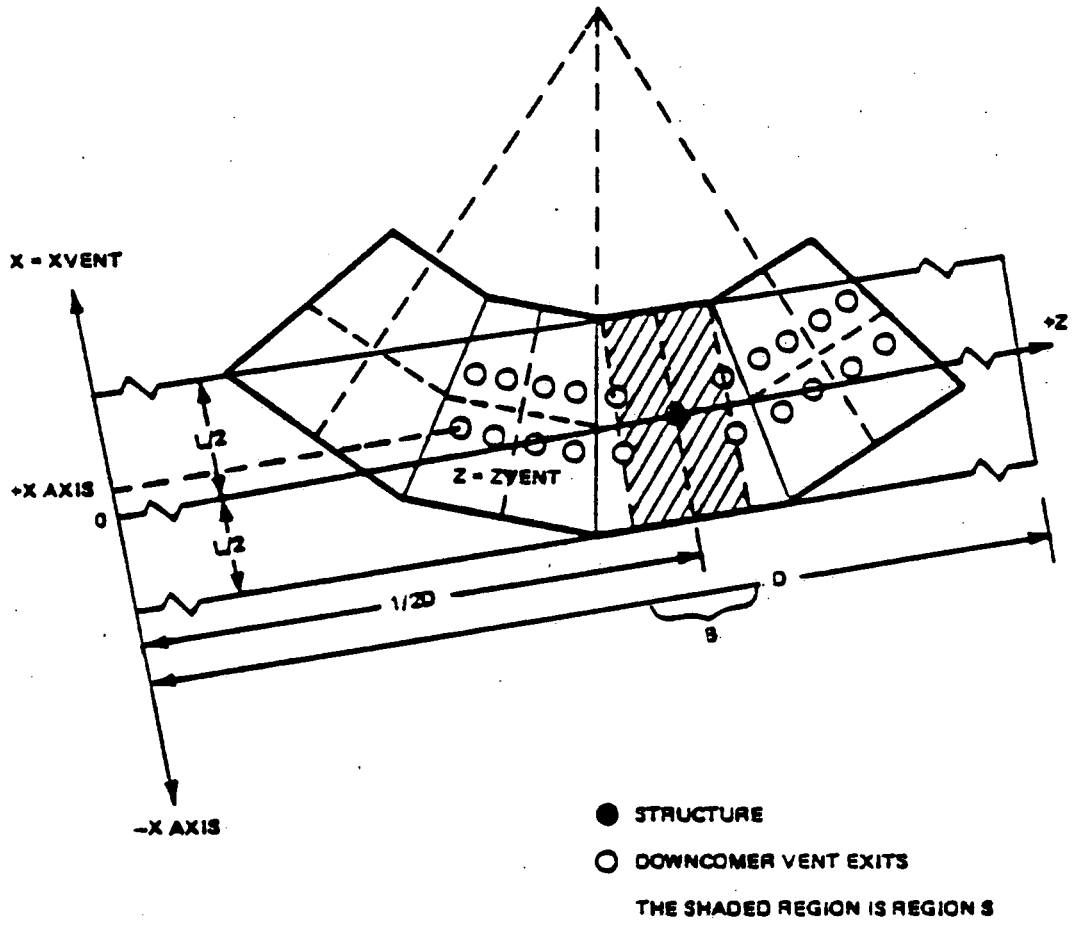

FCOM84.07-05

Figure 3-2

RECTANGULAR CELL MODELING FOR PLANTS WITH 96 DCS C.O. AND CHUGGING (CELL B)

nutech ENGINEERS

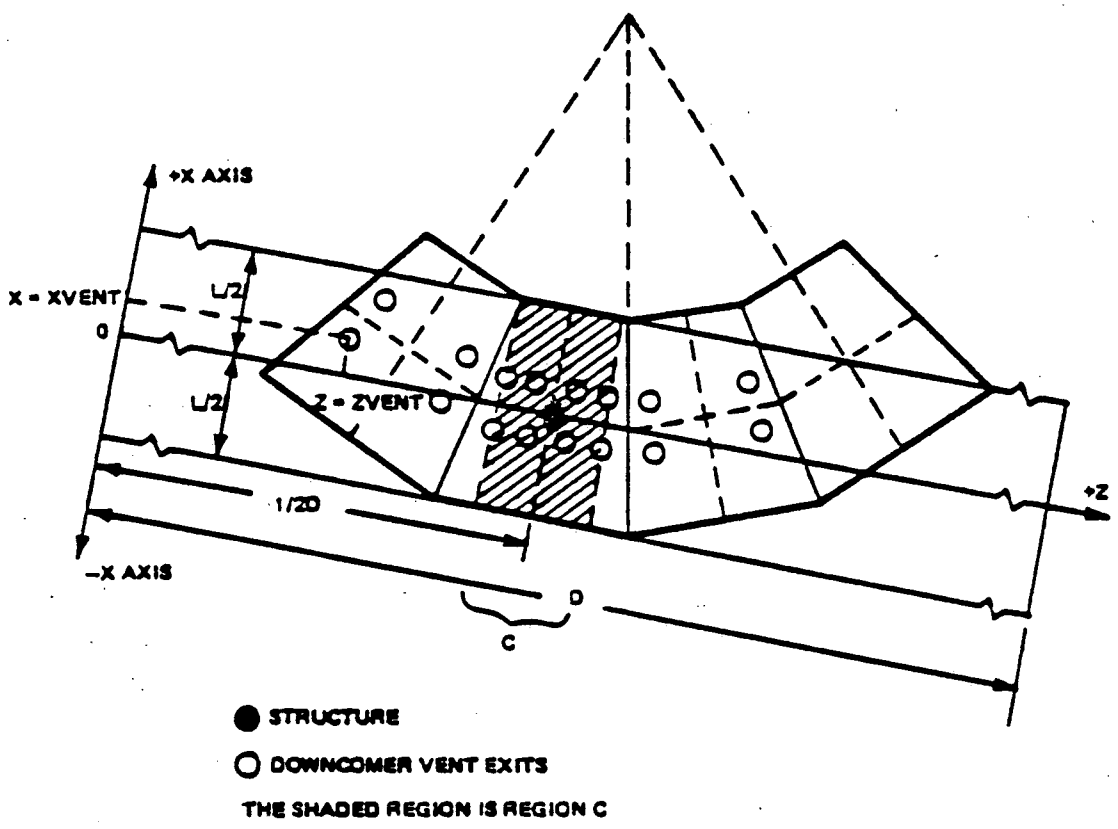

Figure 3-3

RECTANGULAR CELL MODELING FOR PLANTS WITH 96 DCS C.O. AND CHUGGING (CELL C)

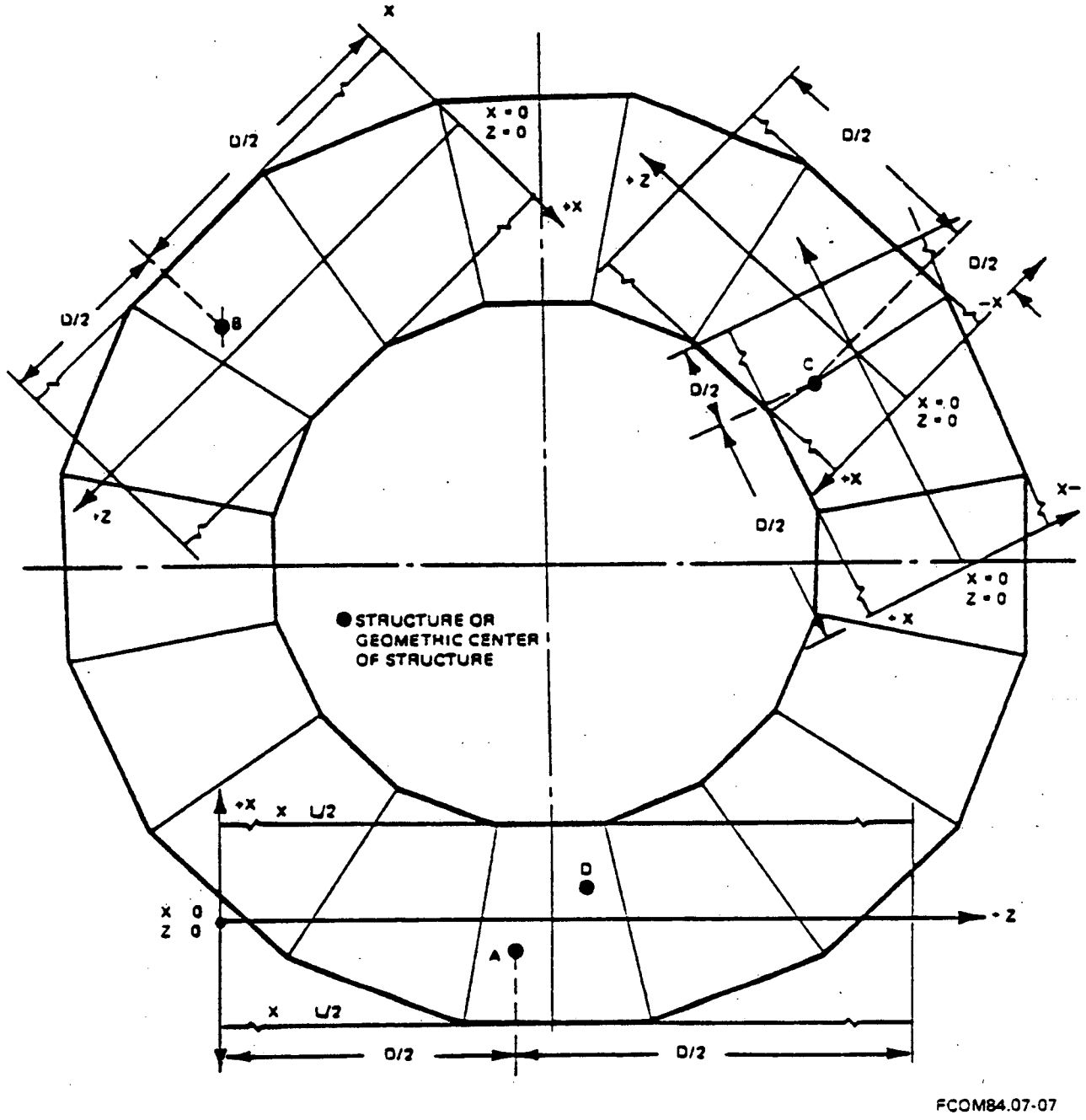

FCOM84.07-07

Figure 3-4

RECTANGULAR CELL MODELING -
SRV AIR BUBBLES

nutech ENGINEERS

nutech
ENGINEERS

NRC QUESTION ON MONTICELLO PUAR STRUCTURAL RESPONSE

Item 4: Multiple downcomer lateral loads (Section 1-4.1.8.2) are based on non-exceedance probabilities that differ from that specified by NUREG-0661. The difference between the load based on the alternate procedure and that based on the Acceptance Criteria is strongly dependent on the number of downcomers participating in the loading. For instance, the FSTF load/downcomer for 6 downcomers based on the Monticello non-exceedance probability is 1.67 kips (Table 3-2.2-16), while the NUREG-0661 load is 1.96 or 17% higher. The justification provided in Appendix A response to question 4 is not totally convincing. In order to ascertain the importance of the issue, provide the following information:

a) The number of downcomers used to establish the critical loads on the vent header under SBA-II conditions (Table 3-2.5-5).

b) The contribution of chugging downcomer lateral loads to the vent header membrane stresses (Table 3-2.5-5).

RESPONSE TO ITEM 4

According to Section 3.9.2 of NUREG-0661, single downcomer maximum resultant static equivalent load (RSEL) is sufficiently conservative to assure the integrity of the downcomer and its intersection with the vent header during chugging. However, a very conservative assumption of two downcomers in a pair loaded in the same direction (during a pool-chug) was used to establish the critical chugging load on the vent header at the downcomer intersection under SBA-II condition (PUAR Table 3-2.5-5).

Curves in Figure 3.9-3 of NUREG-0661 for multiple downcomer chugging load start with 5 downcomers as the lowest number of downcomers having the force in the same direction. Also, section 3.9-2 of NUREG-0661 states that because of the short duration of the chugging lateral loads, their somewhat random occurrence in time, and their random direction when they occur, the probability that the two downcomers in a pair are simultaneously loaded in a reinforcing manner (force in the same direction) is very small. To obtain the loads for two downcomers, the curves in Figure 3.9-3 of NUREG-0661 were conservatively extrapolated. The load magnitude per downcomer from this conservative extrapolation came out as 10.74 kips (PUAR Table 3-2.2-18). Thus, a total of 21.48 kips (2 times 10.74) load was conservatively applied in a pair as compared to the maximum single downcomer RSEL of 11.81 kips (PUAR Figure 3-2.2-15).

The contribution of the above two downcomer lateral load of 21.48 kips to the total vent header membrane stress for SBA-II of the downcomer intersection (PUAR Table 3-2.5-5) is 51 percent. The total stress for SBA-II load combination in this table is 28.73 kips. The allowable stress at this location was conservatively taken as 1.5 Sm_c (28.95 ksi). However, NUREG-0661, Figure 4.3-1 allows a one-third increase in allowable for this load combination (Footnote 4 on page 160 of NUREG-0661) based on the limit analysis. Thus, allowable stresses are 1.3 times the 28.95 ksi reported in the PUAR resulting in a considerable margin in actual stresses over the allowables.

nutech
ENGINEERS

NRC QUESTION ON MONTICELLO PUAR STRUCTURAL AND PIPING RESPONSE

Item 5: SRV drag loads on SRV lines, T-quenchers and their supports, downcomers, vent header support columns and internal piping and pipe supports are based on the use of calibration factors developed from in-plant tests held at Monticello in 1977 and 1980. Describe in detail how these calibration factors are applied. Give numerical values of these "factors" for the major structural components. Describe how extrapolation is made from test conditions to design conditions, especially those involving multiple valve discharges.

RESPONSE TO ITEM 5

The SRV drag load calibration factors for the SRV (wetwell) piping, ramshead, T-quencher, T-quencher support beam, and elbow support beam structures are applied in the manner described below.

1. Prototype piping models were analyzed for the design condition SRV thrust loading, SRV drag loads, and SRV pressure loads using the PISTAR computer code.

2. The stress combinations for the above loads were evaluated using the absolute sum method along with appropriate stress intensification factors. These design condition combined stresses were calculated at various locations on the SRV wetwell piping, ramshead, T-quencher, T-quencher support beams, and elbow support beams. (SRV thrust and pressure load stresses were calculated for all 8 SRVD lines while SRV drag load stresses were calculated only for line SRV-24.)

3. The combined design condition maximum stresses for the SRV wetwell piping, ramshead, T-quencher, T-quencher support beam, and elbow support beam were developed by combining:

   (a) Design condition maximum stresses due to SRV thrust and pressure for each piping location for all 8 of the SRVD lines, and

   (b) Design condition SRV drag load stresses from the SRV-24 wetwell analytical model.

4. These maximum combined stresses (from 3 above) were scaled down by the in-plant test calibration factors, and were reported as the maximum stresses for SRV loading. These scaled-down stresses were then used in the Mark I load combinations per Table 5-2 of the PUAAG.

   The calibration factors for the vent header supports and downcomers were applied in a similar manner. The scaled-down stresses were then used in the Mark I load combinations.

   Numerical values of the calibration factors are as follows:

Structural Component	Calibration Factor
SRV Wetwell Piping	1.59
Ramshead	2.49
T-Quencher	3.58
T-Quencher Support Beam	2.49
Elbow Support Beam	3.82
Vent Header Supports	2.05
Downcomers	2.05

No direct extrapolation from test condition to design condition was specifically necessary. The calibration factors were derived

at test conditions and then applied to design conditions as permitted by NUREG 0661, Section 2.13.9. The design condition loads were calculated with the same techniques as those used to calculate the test condition loads. The only difference was in the system parameters (temperature, pressure, etc.). Design loads calculated included consideration of multiple valve actuation.

nutech
ENGINEERS

NRC QUESTION ON MONTICELLO PUAR

PIPING RESPONSE

ITEM 6: Footnotes in Tables 5-2.2-9 and 5-2.2-12 appear to refer to tables of source amplitudes that are inconsistent with text. Clarify whether footnotes are incorrect or the tables mislabeled.

RESPONSE TO ITEM 6

Footnotes in Tables 5-2.2-9 and 5-2.2-12 that refer to tables of source amplitude are mislabeled. The correct tables for source amplitudes for DBA CO (listed a Table 5-2.2-9) and chugging (listed as Table 5-2.2-12) should be Table 5-2.2-10 and Table 5-2.2-13, respectively.

nutech
ENGINEERS

NRC QUESTION ON MONTICELLO PUAR
PIPING RESPONSE

ITEM 7: Are all SRVDL's in Monticello Configured identically? If not, which line was chosen for detailed analysis in the PUAR, and on what basis was it chosen?

RESPONSE TO ITEM 7

All 8 SRVDL's in the drywell area have different piping and support configurations. All 8 SRVDL's in the wetwell area (that portion of SRVDL piping from the vent line penetration downwards) are identical. All 8 SRVDL's were analyzed (4 full models, as outlined in Section 4-2.4.1) in the PUAR for loads shown in Table 5-2.4-2. One SRVDL including both wetwell and drywell portions was analyzed for hydrodynamic and other loads, as listed in Table 5-2.4-2.

The basis for choosing SRV-24 was that this was the line instrumented in the SRV in-plant tests during 1977 and 1980.

nutech
ENGINEERS

NRC QUESTION ON MONTICELLO PUAR
PIPING RESPONSE

ITEM 8: Provide calculations demonstrating conformance to the 10% rule of Section 3.1.1 of the Plant-Unique Analysis Report for Small Bore Piping Systems in the Monticello Plant that were exempted from analysis.

RESPONSE TO ITEM 8

Section 3.1.1 of Volume 6 of the PUAR describes the methods used to implement the 10% rule. The rule calls for the calculation of piping stresses due to LDR loads for all load combinations for service levels B, C and D. Starting from the torus attachment point, these piping stresses for all service levels at critical piping locations were compared to allowables. The point beyond which these stresses for all load cases were less than 10% of their respective allowables was the "10%" point.

The listing of all Monticello TAP systems along with the distances to the 10% point are shown below:

PIPING LINE	PENETRATION NO.	DISTANCE FROM TORUS PENETRATION TO 10% POINT
HPCI TE	X-221	86 ft.
RCIC TE	X-212	33 ft.
PCAC-CP4	X-218	16,21,13,32 ft.
PCAC-CP5	X-205	23 ft.
RHR and Core Spray Loop A	X-210B, X-211B	70,57,68,52 ft.
RHR and Core Spray Loop B	X-210A, X-211A	56,45,25,37,33 ft.
All 6 suction lines off suction header	X-224A, X-224B, X-225, X-226A, X-226B, X-227	24,30,24,16 ft.

nutech ENGINEERS

nutech
ENGINEERS

NRC QUESTION ON MONTICELLO PUAR STRUCTURAL RESPONSE

ITEM 9: With reference to Table 5.2-2 of the PUA report (1), provide and justify the reasons for not considering load cases which include loads such as pool swell and safe shutdown earthquake.

RESPONSE TO ITEM 9

Load combinations involving pool swell and safe shutdown earthquake (SSE) are primarily service level C load combinations where allowable stresses are significantly higher than for service level B.

Comparison of these loads (pool swell and SSE) against condensation oscillation (C.O.), chugging, and SRV loads showed that the service level B load combinations involving C.O., chugging, and SRV completely bound the service level C load combinations involving pool swell and SSE. The increase in allowable stress from service level B to C far exceeds any difference between these loads, thereby eliminating any need to evaluate these load combinations.

nutech
ENGINEERS

NRC QUESTION ON MONTICELLO PUAR
PIPING RESPONSE

ITEM 10: With respect to Section 5.2.1 of the PUA report, provide and justify the reasons for considering the reduction factor of 1.87 to be the representative value for SRV discharge loads for all TAP lines when this reduction factor was determined, using test results for the Monticello RCIC line only.

RESPONSE TO ITEM 10

The PUA is misleading in that it states that the reduction factor of 1.87 was used for all TAP lines. Acutally the reduction factor was only utilized for selected systems and components. The specific details are listed below:

Piping -- The reduction factor for SRV was selectively used only for the RCIC turbine exhaust system of the torus attached piping. This is justified since test results are available for the RCIC system.

Penetration -- The 1.87 reduction factor was used for both RCIC and HPCI turbine exhaust penetrations because of the geometric similarities of their internal piping and structures.

nutech
ENGINEERS

NRC QUESTION ON MONTICELLO PUAR STRUCTURAL AND PIPING RESPONSE

ITEM 11: Tables 3.5-1, 3.5-2, and 5.5-4 of the PUA report (1) indicate that the calculated values of certain stresses are equal to the respective allowables. Indicate conservatisms in the analysis to show that these calculated values would not be exceeded if the concerns expressed in Items 9 and 10 really have a significant effect on the results or if a different analytical approach were to be used.

RESPONSE TO ITEM 11

The stresses shown in the referenced tables are calculated utilizing loads developed in accordance with the LDR and analytical methods, both defined in the PUAR and in accordance with the PUAAG. As such, the stress results, as they are less than code allowables, meet the requirements of NUREG-0661.

Although the specific details of the load and analytical conservatisms are not quantified here, Section 1-1.4 of the PUAR contains a description of some of the conservatisms inherent in the plant unique analysis. It is felt that the small margins to code allowables do not require additional justification as there is conservatism in the calculated stress results and the code allowables themselves are conservatively determined.

nutech
ENGINEERS

NRC QUESTIONS ON MONTICELLO PUAR

PIPING RESPONSE

ITEM 12: The computer code CMDOF has been used in the torus attached piping analysis for all plants that utilized NUTECH as their contractor. With regard to the code provide the following information:

1) Theoretical background of CMDOF computer program
2) Program verification
3) Applicability of the computer program to the torus attached piping analysis.

RESPONSE TO ITEM 12:

1) The NUTECH computer program CMDOF utilized as the major building block, the Structural Mechanics Associates (SMA) developed program, CMDOF. This program was developed during the MK I Program for use by the Mark I Owners. The theoretical background for the coupling technology is contained in the SMA Report on CMDOF. The sections of this report covering the technical basis are included as Attachment A.

2) The computer program CMDOF was verified by SMA using several problems of differing complexity. Listed below are parameters for the four problems.

EXAMPLE PROBLEM	NUMBER OF DOF's STRUCTURE	EQUIPMENT	NUMBER OF COUPLED DOF's	REMARKS
1	5	4	3	Equipment attached to structure at 3 locations
2	5	2,3,4	4	3 separate equipment models attached to structure
3	12	9	3	3 coupled DOF's at 2 locations
4	1	1	1	Ungrounded equipment

As additional verification of the CMDOF program, an examination of the internal matrices of the coupling program was made by NUTECH. Chosen for examination was the "B-Delta" matrix. This matrix was selected since from it, the possibility for numerical instability, due to mass differences, can be readily determined. The numerical properties of the B-Delta matrix are discussed below, including a description of the physical meaning of the matrix. Three sample matrices are also included to illustrate these properties.

Physical Meaning of the B-Delta Matrix

For a decoupled torus analysis, it is assumed that the torus shell experiences some type of motion, while its decoupled "torus-attached" piping remains undisturbed. The compatibility between the torus and the attached piping is not considered. Equilibrium simply means zero internal reactions between the torus and the piping.

In reality however, the torus and the attached piping are coupled at the penetration point, which has some non-zero internal reactions. These reactions maintain the compatibility between the torus and the piping at the penetration point by eliminating the relative motions resulted from the assumed, decoupled torus analysis.

Thus, the coupling process at the penetration requires a dynamic flexibility matrix, which is the so-called B-Delta matrix in the CMDOF program. The coefficients of the matrix, by definition, are the relative (differential) accelerations between the decoupled torus and the decoupled "attached" piping due to unit and opposite (internal) reactions at the penetration. Using the matrix, we can then calculate the magnitude of internal reactions required to maintain compatibility.

Numerical Properties of the B-Delta Matrix

As a matrix of dynamic flexibililty coefficients, the B-Delta matrix is, in matrix terminology, symmetric (due to the dynamic reciprocal law in structural mechanics) and positive definite (due to the stability of the torus and attached piping).

For torus attached piping applications, the diagonal terms of the matrix are quite uniform in magnitude. In order to illustrate this, three typical piping systems analyzed with CMDOF were reviewed and their "B-Delta" matrices extracted. These three matrices were chosen to represent the range of piping systems analyzed in the MK1 program. Figure 1 is the matrix for a 2" turbine drain line. This was typically the smallest line analyzed using full coupling techniques. Figure 2 contains the matrix for an 8" pressure relief line and figure 3 contains the matrix for a 24" RHR suction line, the largest piping analyzed.

It can be seen that the diagonal terms of the three sample matrices are within 4-5 orders of magnitude (maximum 1-13,500). The large digital computers with 60 bits per word and 15 digits of accuracy used for CMDOF analysis will not suffer numerical problems with this range. This is especially true for the B-Delta matrix found in a torus-attached piping application where the matrix size, i.e., the number of coupling degrees of freedom, is small and far less than typically large structural stiffness matrices.

3) The CMDOF computer program was utilized for large bore torus attached piping analysis. In certain cases the coupling analysis was utilized for small bore lines (2" diameter).

The use of coupling techniques for small bore piping was infrequent as the benefits of coupling were quite small. Conversely, coupling for large bore piping exhibited significant coupling benefits.

To illustrate the effect of pipe size on coupling, four typical piping systems were examined and the coupled and uncoupled time histories plotted together. These time histories include both the smallest (2") and larger (20") systems analyzed. Listed below are the figure numbers and the corresponding line size.

Figure 4-8	2" diameter
9-13	4" diameter
14-18	6" diameter
19-21	20" diameter

These plots confirm the expected variation of coupling benefit with pipe size.

ATTACHMENT A

2. TECHNICAL BASIS

2.1 ASSUMPTIONS

1. At the attachment point, the structure uncoupled and coupled acceleration time histories and the equipment reaction time history for all degrees-of-freedom are assumed to vary linearly between time steps. This assumption is common to many dynamic analysis programs and the time step size for this coupling program does not have to be any smaller than for most other dynamic analysis programs. A time step equal to (0.1/f) where f is the highest natural frequency of interest is generally considered adequate.

2. Both the structure and the attached equipment are considered to behave linearly elastic. Superposition is used extensively in this program.

3. Sufficient structural and equipment modes are included to accurately model the structure and equipment at the degree-of-freedom (dof) of interest.

2.2 COMPATIBILITY AND SUPERPOSITION

Figure 2-1 illustrates an uncoupled structure model and uncoupled equipment models which are attached to the structure at a series of different nodes with one dof (dof) of coupling per node. Another model which would be just as valid for use in conjunction with the theory which follows is one in which the equipment is attached to the structure at only a couple of nodes but there are multiple degrees of coupling at each attachment node. In the following discussion, there are assumed to be NC coupled dof between the structure and equipment.

As shown in Figure 2-1, the uncoupled structure is subjected to an input force loading $F(t_i)$ which in the absence of the attached equipment results in a series of uncoupled accelerations $a_{u_j}(t_i)$ for each attachment mode at time t_i. By knowing the modal characteristics of the uncoupled structure and uncoupled equipment models (frequency, eigenvector, participation factor for each of the NC attachment dof) the coupling reaction $R_j(t_i)$ for each dof applied by the equipment on the structure at time t_i can be determined from the coupled accelerations a_{c_j} defined at all previous time steps t_0 through t_{i-1}. This reaction $R_j(t_i)$ on the uncoupled structure model results in the structural response acceleration $a_{R_j}(t_i)$ at dof j where $a_{R_j}(t_i)$ is the acceleration at time t_i due to the equipment reaction R_j for all previous times considering the contributions of all NC attachment dof between the equipment and structure. By using superposition, the coupled acceleration of the attachment point for dof j is given by:

$$a_{c_j}(t_i) = a_{u_j}(t_i) + a_{R_j}(t_i) \qquad (2.1)$$

Note that $a_{R_j}(t_i)$ is due to the equipment reaction time histories R_k for all coupling DOF through time t_i which, in turn, are due to the coupled acceleration time histories a_{c_j} for all coupled DOF through time t_i.

Compatibility requires that the coupled accelerations $a_{c_j}(t_i)$ and the reactions $R_j(t_i)$ at the attachment points be identical for the structure and attached equipment for every time point t_i. Similarly, superposition requires that Equation 2.1 be satisfied

at every point t_i. At the outset, only the uncoupled response time histories defined by $a_{u_j}(t_i)$ are known at each time point t_i. The essence of this program is to determine the reaction $R_j(t_i)$ and reaction acceleration $a_{R_j}(t_i)$ for all NC attachment dof time point by time point so that compatibility and superposition are satisfied at every time point t_i.

2.3 STRUCTURE RESPONSE DUE TO EQUIPMENT REACTIONS

The reaction acceleration $a_{R_k}(t_i)$ for the structure at the equipment attachment node for dof k can be defined in terms of the reaction forces $R_j(t_i)$ by:

$$a_{R_k}(t_i) = \sum_{j=1}^{NC} \sum_{m=1}^{M_S} PF_{S_{j,m}} \cdot \phi_{S_{k,m}} \cdot \ddot{Y}_{j,m}(t_i) \qquad (2.2)$$

where NC represents the total number of coupling degrees-of-freedom considered, M_S represents the total number of important structure modes, $PF_{S_{j,m}}$ is the uncoupled structure participation factor for mode m associated with an applied unit force/moment at dof j, and $\phi_{S_{k,m}}$ is the structural eigenvector for attachment dof k, for uncoupled structure mode m. The uncoupled structure m-th mode acceleration due to reaction $R_j(t_i)$ at dof j and time t_i is given by:

$$\ddot{Y}_{j,m}(t_i) + 2\lambda_{S_m}\omega_{S_m}\dot{Y}_{j,m}(t_i) + \omega_{S_m}^2 Y_{j,m}(t_i) = -R_j(t_i) \qquad (2.3)$$

where λ_{S_m} is the modal structural damping ratio and ω_{S_m} is the modal angular natural frequency for uncoupled structure mode m.

Given the response at time t_{i-1}, the modal response at time t_i for the attachment node, dof j, can be determined using the Nigam-Jennings technique (Reference 1) as follows:

$$\left.\begin{aligned} Y_{j,m}(t_i) &= Y^*_{j,m}(t_i) + B_{12S_m} \cdot \Delta R_j(t_i) \\ Y^*_{j,m}(t_i) &= A_{11S_m} \cdot Y_{j,m}(t_{i-1}) + A_{12S_m} \cdot \dot{Y}_{j,m}(t_{i-1}) + B_{11S_m} \cdot R_j(t_{i-1}) \\ \dot{Y}_{j,m}(t_i) &= \dot{Y}^*_{j,m}(t_i) + B_{22S_m} \cdot \Delta R_j(t_i) \\ \dot{Y}^*_{j,m}(t_i) &= A_{21S_m} \cdot Y_{j,m}(t_{i-1}) + A_{22S_m} \cdot \dot{Y}_{j,m}(t_{i-1}) + B_{21S_m} \cdot R_j(t_{i-1}) \end{aligned}\right\} \quad (2.4)$$

By substituting Equation 2.4 into Equation 2.3,

$$\left.\begin{aligned} \ddot{Y}_{j,m}(t_i) &= \ddot{Y}^*_{j,m}(t_i) - \Delta R_j(t_i) \cdot \left[1 + 2\lambda_{S_m}\ \omega_{S_m}\ B_{22S_m} + \omega^2_{S_m}\ B_{12S_m}\right] \\ \ddot{Y}^*_{j,m}(t_i) &= -R_j(t_{i-1}) - 2\lambda_{S_m}\ \omega_{S_m}\ \dot{Y}^*_{j,m}(t_i) - \omega^2_{S_m}\ Y^*_{j,m}(t_i) \end{aligned}\right\} \quad (2.5)$$

where $R_j(t_{i-1})$ represents the equipment reaction for attachment dof i at the previous time point t_{i-1}, and $\Delta R_j(t_i)$ represents the change in reaction for attachment dof j during the time interval from t_{i-1} to t_i. The change in reaction $\Delta R_j(t_i)$ is unknown because the equipment solution has not been completed through time t_i. However, the reaction $R_j(t_{i-1})$ for the previous time point is known so that the quantities $Y^*_{j,m}(t_i)$, $\dot{Y}^*_{j,m}(t_i)$, $\ddot{Y}^*_{j,m}(t_i)$ can be evaluated for all the attachment dof for each structure mode m at time t_i. Using $\ddot{Y}^*_{j,m}(t_i)$ the reaction acceleration $a_{R_k}(t_i)$ at dof k for all NC dof can be determined using Equation 2.2 as follows:

$$\ddot{d}^*_{R_k}(t_i) = \sum_{j=1}^{NC} \sum_{m=1}^{M_S} PF_{S_{j,m}} \cdot \phi_{S_{k,m}} \cdot \ddot{Y}^*_{j,m}(t_i) \quad (2.6)$$

The reaction acceleration $a^{*}_{R_k}(t_i)$ represents the reaction acceleration for the attachment node, dof k, that would result if no change in reactions occurred between time t_{i-1} and t_i (i.e., $\Delta R_j(t_i) = 0$).

The change in reaction acceleration for dof k, $a_{\Delta R_k}(t_i)$ due to the change in reaction $\Delta R_j(t_i)$ as obtained from Equations 2.2 and 2.5 is:

$$a_{\Delta R_k}(t_i) = \sum_{j=1}^{NC} A_{\Delta S_{k,j}} \cdot \Delta R_j(t_i) \qquad (2.7)$$

where:

$$A_{\Delta S_{k,j}} = - \sum_{m=1}^{M_S} PF_{S_{j,m}} \cdot \phi_{S_{k,m}} \left[1 + 2\lambda_{S_m} \omega_{S_m} B_{22S_m} + \omega^2_{S_m} B_{12S_m} \right] \qquad (2.8)$$

The quantity $A_{\Delta S_{k,j}}$ represents the change in the structure reaction acceleration at dof k, due to a unit change in the reaction/moment at attachment dof j during the time step and is independent of the structural response or time step. This quantity simply depends upon the uncoupled structure modal properties and the time step size Δt.

The total reaction acceleration for attachment dof k at time t_i is given by:

$$a_{R_k}(t_i) = a^{*}_{R_k}(t_i) + a_{\Delta R_k}(t_i) \qquad (2.9)$$

The coupled acceleration for attachment dof K as obtained from Equation 2.1 is thus:

$$a_{C_k}(t_i) = a^*_{CS_k}(t_i) + a_{\Delta R_k}(t_i) \tag{2.10}$$

where:

$$a^*_{CS_k}(t_i) = a_{u_k}(t_i) + a^*_{R_k}(t_i) \tag{2.11}$$

The Nigam-Jennings coefficients used in Equations 2.4 and 2.5 for calculating the modal structural response are derived from the coefficients in Reference 1 and are as follows:

$$
\begin{aligned}
A_{11} &= \omega^2 B_{11} + 1 \\
A_{12} &= -B_{21} \\
A_{21} &= \omega^2 B_{21} \\
A_{22} &= A_{11} + 2\lambda\omega B_{21} \\
B_{11} &= \Delta t_i \; B_{22} \\
B_{12} &= -e^{-\lambda\omega\Delta t_i}\left[\left(\frac{2\lambda^2-1}{\omega^3\Delta t_i}\right)\frac{\sin\omega_D\Delta t_i}{\omega_D} + \frac{2\lambda}{\omega^3\Delta t_i}\cos\omega_D\Delta t_i\right] - \\
&\quad \frac{1}{\omega^2} + \frac{2\lambda}{\omega^3\Delta t_i} \\
B_{21} &= -e^{-\lambda\omega\Delta t_i}\left[\frac{\sin\omega_D\Delta t_i}{\omega_D}\right] \\
B_{22} &= e^{-\lambda\omega\Delta t_i}\left[\frac{\cos\omega_D\Delta t_i}{\omega^2\Delta t_i} + \left(\frac{\lambda}{\omega\Delta t_i}\right)\frac{\sin\omega_D\Delta t_i}{\omega_D}\right] - \frac{1}{\omega^2\Delta t_i}
\end{aligned}
\qquad (2.12)
$$

where the damped modal natural frequency ω_D is given by

$$\omega_D = \omega\sqrt{1-\lambda^2} \qquad (2.13)$$

Note that all of the coefficients are defined in terms of B_{12}, B_{21}, and B_{22}. Further note that when the product $\omega\Delta t_i$ is small, both B_{12} and B_{22} are obtained by the subtraction of two nearly equal numbers. On a computer with seven to eight significant figure accuracy it has been found that the coefficients B_{12}, and B_{22} can be evaluated both faster and more accurately using a series expansion in lieu of Equation 2.12 whenever

$$\omega\Delta t_i < 0.3$$

The series expansion used is

$$
\begin{aligned}
B_{12} &= -e^{-\lambda\omega\Delta t_i}\left(\frac{\Delta t_i^2}{6}\right)\left[1 + \frac{\lambda\omega\Delta t_i}{2} + \frac{(4\lambda^2-1)\;(\omega\Delta t_i)^2}{20} + \right. \\
&\quad \left. \frac{\lambda(3\lambda^2-1)\;(\omega\Delta t_i)^3}{60} + \frac{(1-5\lambda^2+9\lambda^4)\;(\omega\Delta t_i)^4}{840}\right] \\
B_{22} &= -e^{-\lambda\omega\Delta t_i}\left(\frac{\Delta t_i}{2}\right)\left[1 + \frac{\lambda\omega\Delta t_i}{3} + \frac{(2\lambda^2-1)(\omega\Delta t_i)^2}{12} + \right. \\
&\quad \left. \frac{\lambda(2\lambda^2-1)(\omega\Delta t_i)^3}{60} + \frac{(1-3\lambda^2+3\lambda^4)\;(\omega\Delta t_i)^4}{360}\right]
\end{aligned}
\qquad (2.14)
$$

2.4 UNCOUPLED EQUIPMENT RESPONSE TO ATTACHMENT POINT REACTION

Using a development similar to that shown for the structure in Section 2.3, the following definitions are possible. The reaction acceleration $a_{ce_k}(t_i)$ for dof k at the corresponding equipment attachment node is identical to the coupled acceleration $a_{c_k}(t_i)$. Thus, the coupled acceleration at dof k can be defined in terms of the coupling reaction forces $R_j(t_i)$ by:

$$a_{c_k}(t_i) = -\sum_{j=1}^{NC} \sum_{m=1}^{M_E} PF_{E_{j,m}} \cdot \phi_{E_{k,m}} \cdot \ddot{Z}_{j,m}(t_i) \qquad (2.15)$$

where NC represents the total number of degrees-of-freedom considered at the equipment attachment nodes, M_E represents the total number of important equipment modes, $PF_{E_{j,m}}$ is the uncoupled equipment participation factor for mode m associated with an applied unit force/moment at attachment dof j, and $\phi_{E_{k,m}}$ is the equipment eigenvector for attachment dof k for uncoupled equipment mode m. The uncoupled equipment m-th mode acceleration for an applied reaction $R_j(t_i)$ at dof j and time t_i is given by:

$$\ddot{Z}_{j,m}(t_i) + 2\lambda_{E_m} \omega_{E_m} \dot{Z}_{j,m}(t_i) + \omega^2_{E_m} Z_{j,m}(t_i) = -R_j(t_i) \qquad (2.16)$$

where λ_{E_m} is the modal equipment damping ratio and ω_{E_m} is the modal angular natural frequency for uncoupled equipment mode m.

A set of equations identical to Equations 2.4 and 2.5 may be written for the equipment by making the following substitutions. All letters Y, $\dot{Y}$, $\ddot{Y}$, Y^*, $\dot{Y}^*$, and $\ddot{Y}^*$ must be replaced by Z, $\dot{Z}$, $\ddot{Z}$, Z^*, $\dot{Z}^*$, and $\ddot{Z}^*$ respectively while keeping all subscripts the same. All Nigam-Jennings coefficients for the structure A_{11S}, A_{12S}, ... B_{22S} must be replaced by the analogous equipment Nigam-Jennings response coefficients A_{11E}, A_{12E}, ... B_{22E}. Interpretation of the resulting equations for the equipment modal accelerations, velocities, and displacements, are similar to those given in Section 2.3 for the uncoupled structure.

Since the quantity $R_j(t_{i-1})$ for the previous time point is known, the quantities $Z^*_{j,m}(t_i)$, $\dot{Z}^*_{j,m}(t_i)$, $\ddot{Z}^*_{j,m}(t_i)$ can be evaluated for all NC attachment dof for each equipment mode m at at time t_i. Using $\ddot{Z}^*_{j,m}(t_i)$, the reaction acceleration $a^*_{ce_k}(t_i)$ can be determined from Equation 2.15 as follows:

$$a^*_{ce_k}(t_i) = -\sum_{j=1}^{NC} \sum_{m=1}^{M_E} PF_{E_{j,m}} \cdot \phi_{E_{k,m}} \cdot \ddot{Z}^*_{j,m}(t_i) \qquad (2.17)$$

The reaction acceleration $a^*_{ce_k}(t_i)$ represents the reaction acceleration for the equipment attachment node, dof k, that would result if no change in reactions occurred between time t_{i-1} and t_i.

The change in the reaction acceleration for dof k, $a_{\Delta c_k}(t_i)$ due to the change in reaction $\Delta R_j(t_i)$ is:

$$a_{\Delta c_k}(t_i) = \sum_{j=1}^{NC} A_{\Delta E_{k,j}} \cdot \Delta R_j(t_i) \qquad (2.18)$$

where

$$A_{\Delta E_{k,j}} = \sum_{m=1}^{M_E} PF_{E_{j,m}} \cdot \phi_{E_{k,m}} \left[1 + 2\lambda_{E_m} \omega_{E_m} B_{22E_m} + \omega_{E_m}^2 B_{12E_m} \right] \quad (2.19)$$

The quantity $A_{\Delta E_{k,j}}$ represents the change in the equipment reaction acceleration at dof k due to a unit change in reaction/moment at attachment dof j during the time step.

The coupled acceleration for dof k is equal to:

$$a_{c_k}(t_i) = a^*_{ce_k}(t_i) + a_{\Delta c_k}(t_i) \quad (2.20)$$

In order to find the quantities $a_{\Delta R_k}(t_i)$ for the structure (Equation 2.7) and $a_{\Delta c_k}(t_i)$ for the equipment (Equation 2.18) for all NC attachment dof, the change in the coupling reactions $\Delta R_j(t_i)$ must be found for all dof at time step t_i. This may be done by setting Equation 2.10 equal to Equation 2.20 and solving for $\Delta R_j(t_i)$. Thus, for time step t_i:

$$\left[B_\Delta \right] \{ \Delta R \} = \{ C \} \quad (2.21)$$

where:

$$\{ \Delta R \} = \left[B_\Delta \right]^{-1} \{ C \} \quad (2.22)$$

$$B_{\Delta_{k,j}} = A_{\Delta S_{k,j}} - A_{\Delta E_{k,j}} . \quad (2.23)$$

$$C_k(t_i) = a^*_{ce_k}(t_i) - a^*_{cs_k}(t_i) \quad (2.24)$$

By Maxwell's Law the displacement of dof k due to a unit force at dof j must equal the displacement at dof j due to a unit force of dof k, therefore the $[B_\Delta]$ matrix must be symmetric. Thus:

$$B_{\Delta_{k,j}} = B_{\Delta_{j,k}} \tag{2.24a}$$

Lack of symmetry is an indication that improper eigenvector values or improper participation factors have been input to the coupling program.

Thus, the change in reaction for each dof j, $\Delta R_j(t_i)$ during the time step are determined from all of the dof accelerations $C_k(t_i)$ corresponding to the difference in the structure and equipment accelerations resulting from no change in the reactions during the time step t_i and the matrix $[B_\Delta]^{-1}$ which is a constant and is independent of the time history analysis.

Once the change in the coupling reactions $\Delta R_j(t_i)$ are known for all NC attachment dof, the coupled acceleration for each attachment dof may be calculated for time step t_i by Equations 2.7 and 2.10. The total coupling reactions for time step t_i, dof j, are then given by:

$$R_j(t_i) = R_j(t_{i-1}) + \Delta R_j(t_i) \tag{2.25}$$

Thus, it is possible to calculate the coupled structural response at time step t_i using the results of the previous time step t_{i-1}. Once the coupled response is known for all NC attachment dof for time step t_i, the analysis can proceed to the next time point t_{i+1} and continue the correction of the uncoupled acceleration time history by marching time point by time point.

1.4 NOTATION

$A_{11E_m}, \cdots, B_{22E_m}$ = Nigam-Jennings coefficients for equipment mode m.

$A_{11S_m}, \cdots, B_{22S_m}$ = Nigam-Jennings coefficients for uncoupled structure mode m.

$a_{c_j}(t_i)$ = Coupled acceleration of structure attachment point degree-of-freedom j at time t_i.

$a_{R_j}(t_i)$ = Reaction acceleration of structure attachment point degree-of-freedom j at time t_i.

$a_{u_j}(t_i)$ = Uncoupled acceleration of structure attachment point degree-of-freedom j at time t_i.

$d_{c_j}(t_i)$ = Coupled displacement of structure attachment point degree-of-freedom j at time t_i.

$d_{u_j}(t_i)$ = Uncoupled displacement of structure attachment point degree-of-freedom j at time t_i.

f_{E_m} = Equipment mode frequency (Hz) for mode m.

f_{S_m} = Equipment mode frequency (Hz) for mode m.

j,k = Attachment point degree-of-freedom numbers.

m = Mode number.

M_E = Total number of equipment modes.

M_S = Total number of structure modes.

NC = Total number of degrees-of-freedom at which coupling is considered between structure and equipment.

$PF_{E_{j,m}}$ = Uncoupled equipment participation factor for mode m associated with an applied unit force/moment at attachment degree-of-freedom j for the equipment attachment node.

$PF_{S_{j,m}}$ = Uncoupled structure participation factor for mode m associated with applied unit force/moment at attachment degree-of-freedom j for the equipment attachment node on the structure.

$R_j(t_i)$ = Coupling reaction acceleration at time t_i for degree-of-freedom j.

$\Delta R_j(t_i)$ = Change in coupling reaction acceleration from time t_{i-1} to time t_i at degree-of-freedom j

t_i = Time at time step i.

$V_{c_j}(t_i)$ = Coupled velocity of structure attachment point degree-of-freedom j at time t_i.

$\ddot{Y}_{m,j}(t_i), \dot{Y}_{m,j}(t_i), Y_{m,j}(t_i)$ = Modal acceleration, velocity, and displacement for uncoupled structure mode m, dof j at time t_i, respectively.

$\ddot{Z}_{m,j}(t_i), \dot{Z}_{m,j}(t_i), Z_{m,j}(t_i)$ = Modal relative acceleration, velocity, and displacement for uncoupled equipment mode m, dof j at time t_i, respectively.

Δt_i	=	Time step size from time t_{i-1} to time t_i.
λ_{E_m}	=	Ratio of m-th equipment mode damping to critical damping.
λ_{S_m}	=	Ratio of m-th structure mode damping to critical damping.
$\phi_{E_{j,m}}$	=	Uncoupled equipment eigenvector for degree-of-freedom j and mode m.
$\phi_{S_{j,m}}$	=	Uncoupled structure eigenvector value for degree-of-freedom j and mode m.
ω_{E_m}	=	Circular natural frequency for equipment mode m.
ω_{S_m}	=	Circular natural frequency for structure mode m.

1	-12.39				
2	-.1609	14.13	(symmetric)		
3	1.827	-2.504	16.19		
4	.0402	.0727	.2508	.1029	
5	-.5180	.0286	-.1699	-.0037	.1093
DOF	1	2	3	4	5

Figure 1

B-Delta Matrix from a 2" HPCI Turbine Drain

nutech ENGINEERS

1	2	3	4	5	6	7	8	9	10	11	12	13	14	15	DOF
-44.14	-7.588	-28.86	1.722	-9.853	.0217	.0026	-.0529	.0002	.0003	.0521	.0208	.1072	-.0056	-.0227	1
	-65.85	7.726	14.87	-1.733	-.0047	-.0025	.0096	-.0007	.0001	-.0273	.0155	-.0331	-.0052	.0050	2
		-24.07	-1.784	-6.703	-.0272	-.0096	-.0475	-.0009	-.0020	-.1008	-.0251	-.1479	.0016	.0235	3
			-4.074	.4701	.0017	.0147	.0064	.0013	.0004	.0062	-.0054	.0101	-.0007	.0016	4
				-2.704	.0177	.0017	.0112	.0004	-.0018	-.0109	-.0008	.0003	.0016	-.0038	5
					-1.287	.0568	-.0706	-.0061	.0360	-.0668	-.0168	-.0983	-.0011	.0049	6
						-.7525	-.1716	.0021	.0063	.0212	.0027	.0352	.0134	.0002	7
							-1.669	-.0150	-.0047	-.1535	-.0330	-.2943	.0010	.0099	8
								-.0049	-.0006	-.0020	-.0016	-.0016	.0006	.0002	9
						(symmetric)			-.0059	.0024	.0007	.0028	.00004	-.0012	10
										-44.83	7.403	27.95	-1.734	-9.851	11
											-65.94	7.512	14.87	1.736	12
												-25.29	-1.809	6.696	13
													-4.077	-.4722	14
														-2.707	15

Figure 2

B-Delta Matrix from an 8" RHR Pressure Relief

nutech ENGINEERS

1	-10.97				
2	-.4010	-8.188	(symmetric)		
3	-.0525	.6121	-1.131		
4	1.061	-.3145	-.6404	-376.9	
5	115.6	-13.57	3.123	33.63	6080.
DOF	1	2	3	4	5

Figure 3

B-Delta Matrix from a 24" RHR Suction

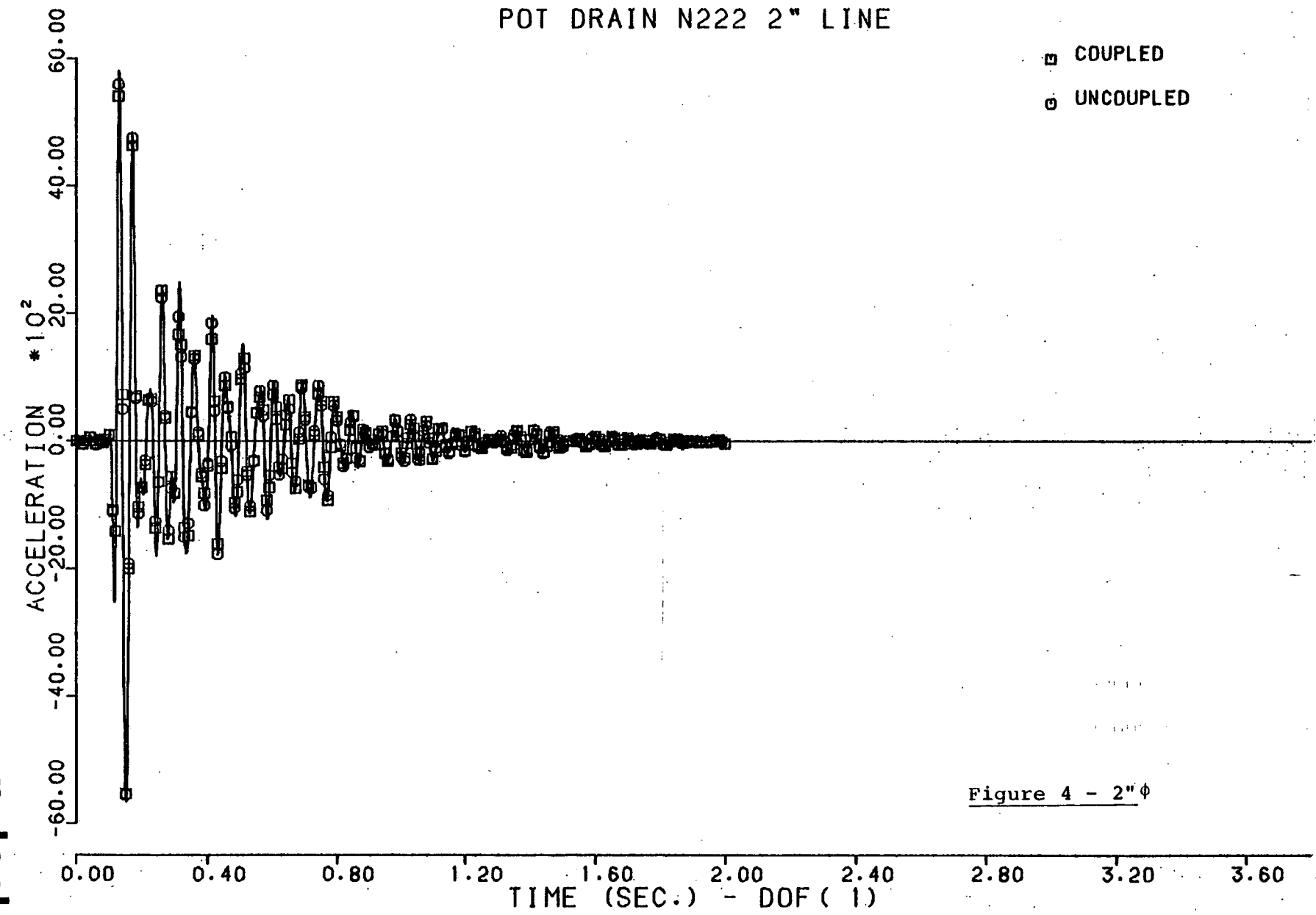

Figure 4 - 2"ϕ

nutech ENGINEERS

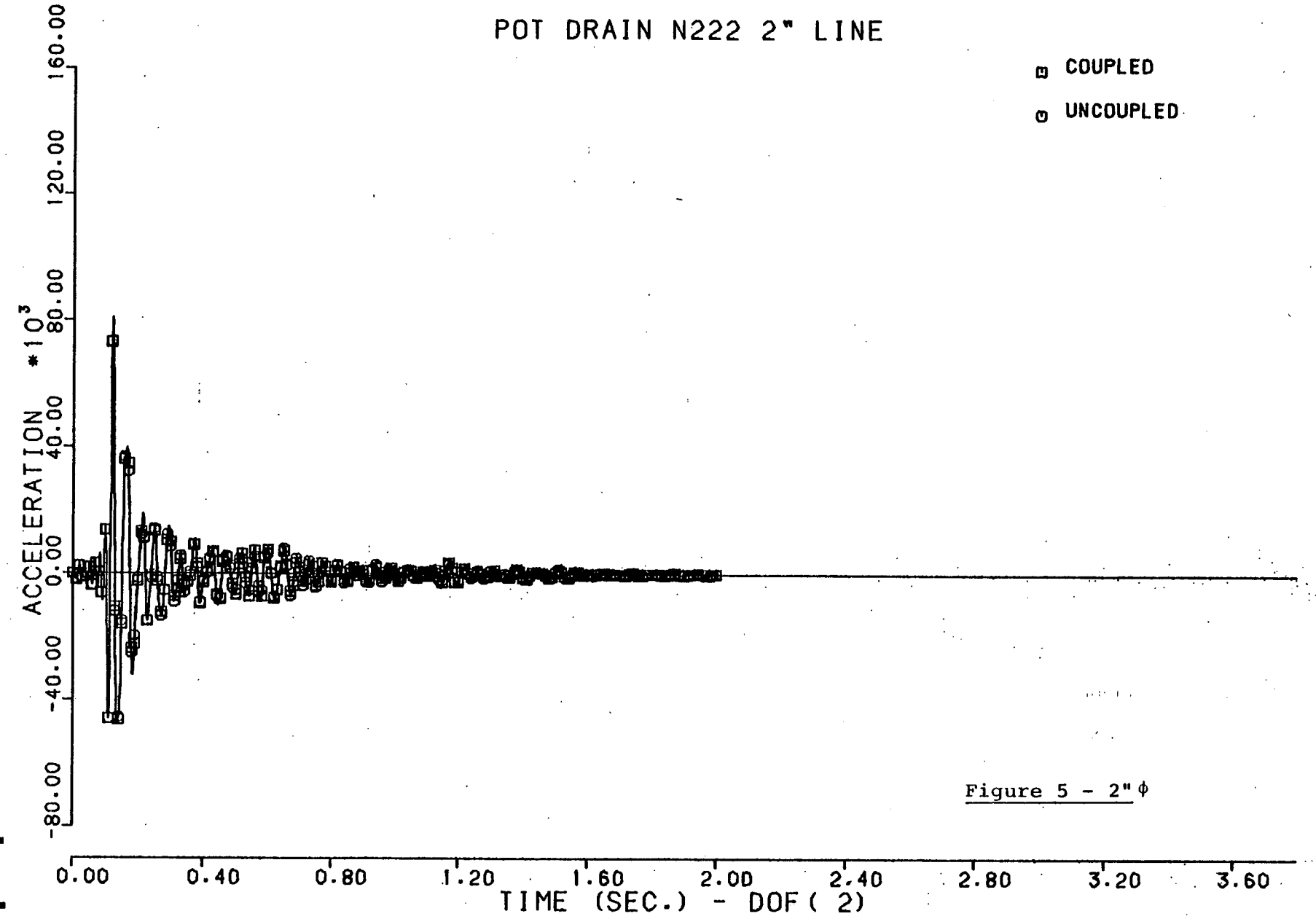

Figure 5 - 2" ϕ

nutech ENGINEERS

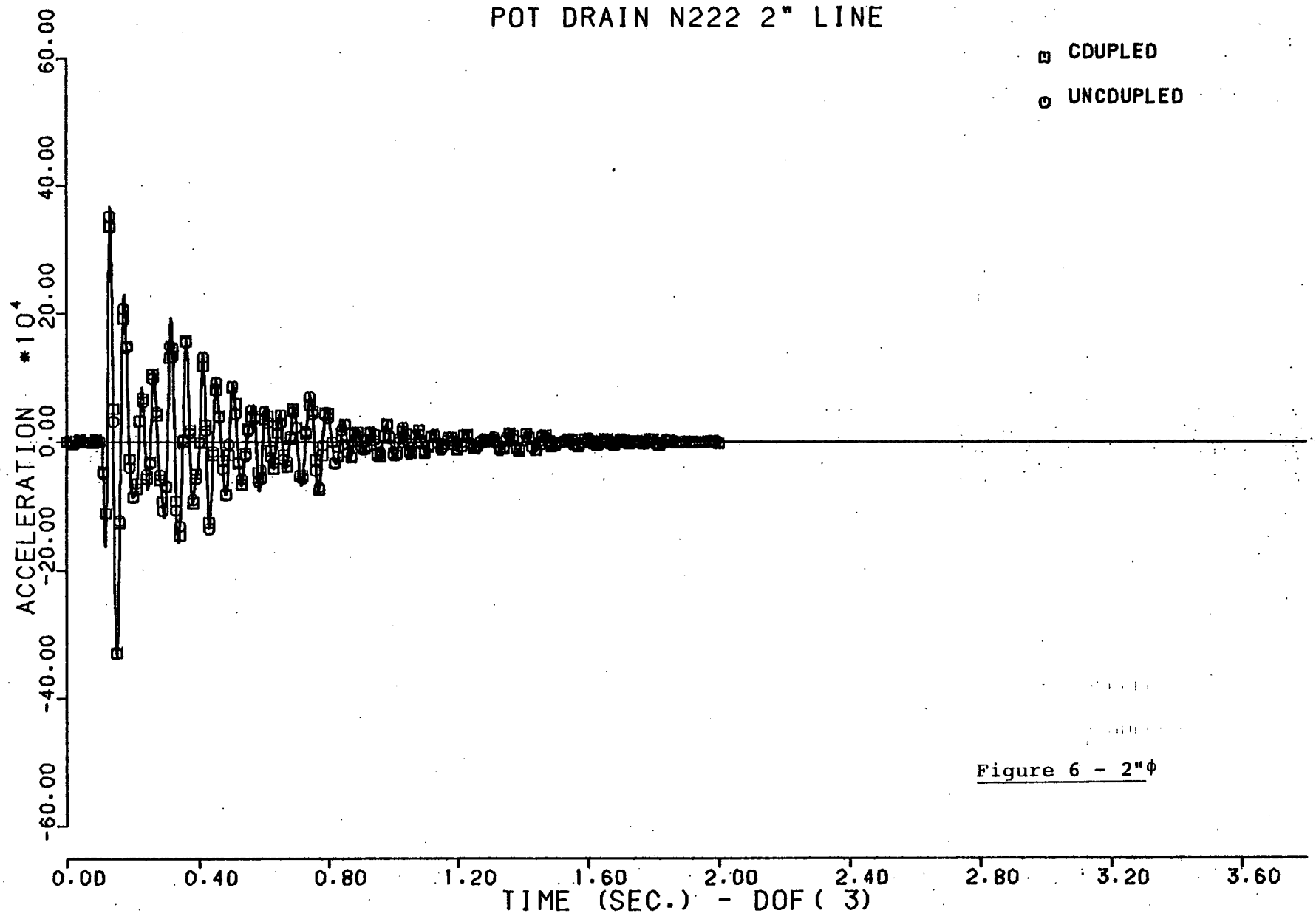

Figure 6 - 2"ϕ

nutech ENGINEERS

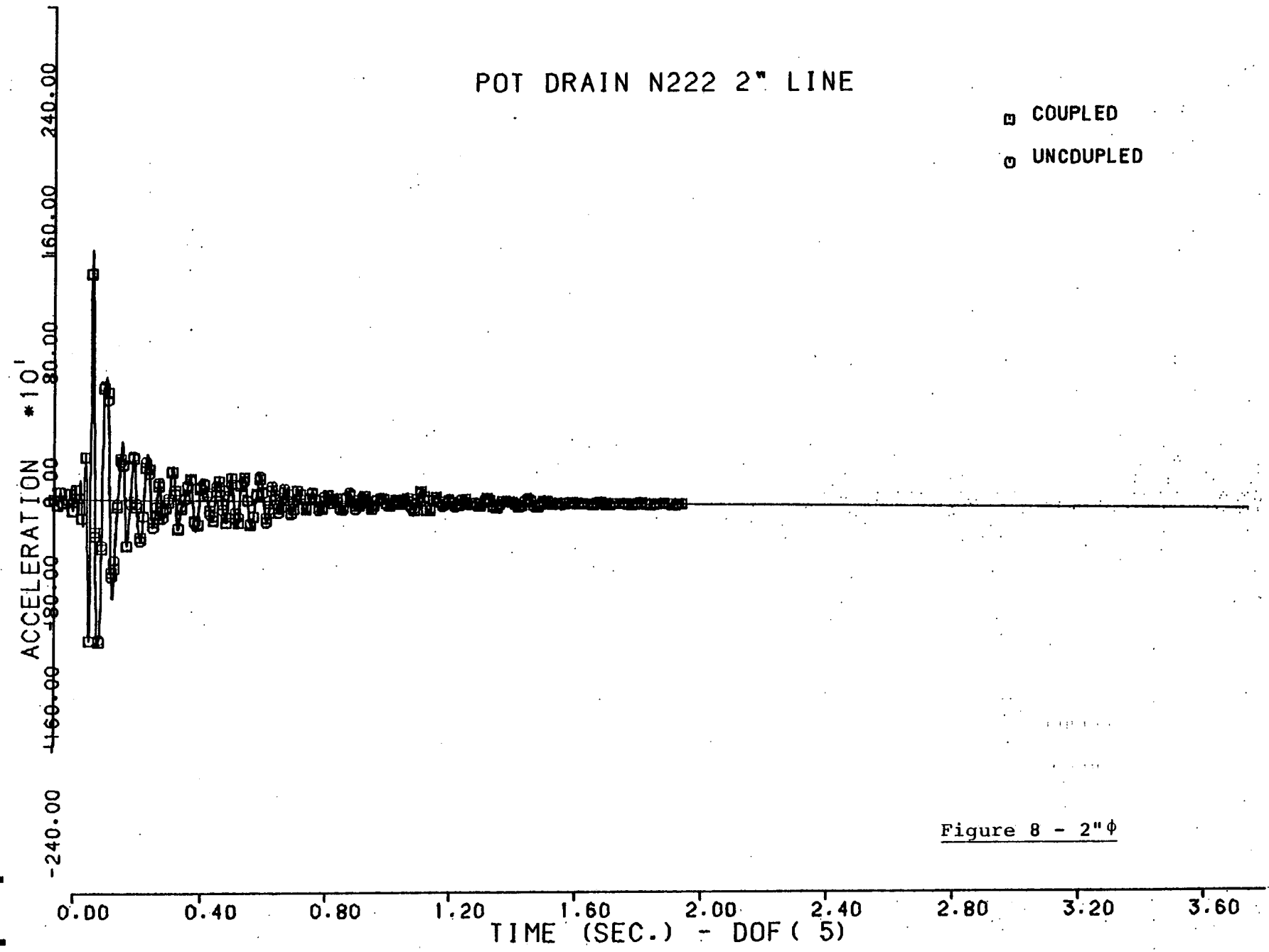

Figure 8 - 2"ϕ

nutech ENGINEERS

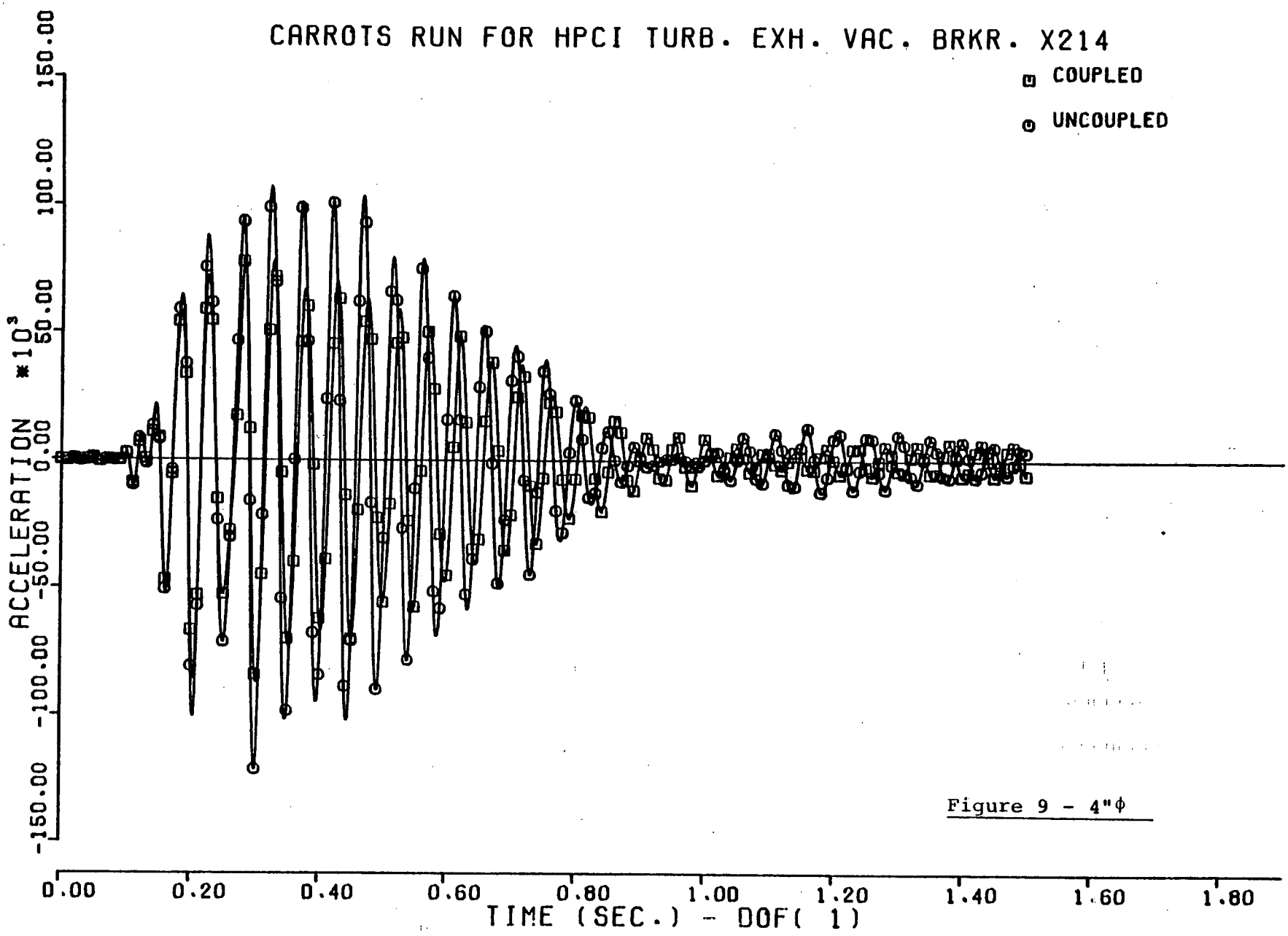

Figure 9 - 4"ϕ

nutech ENGINEERS

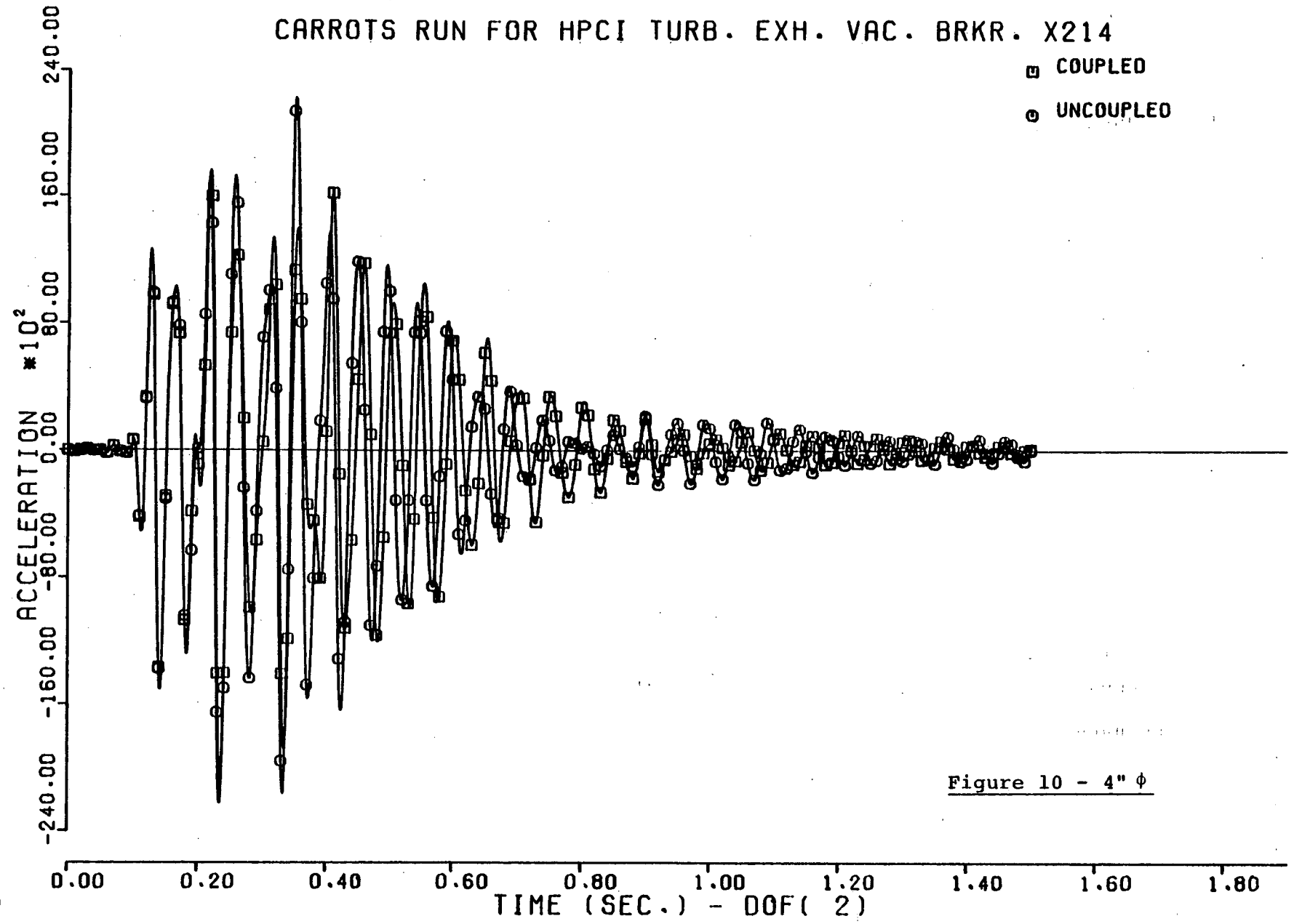

Figure 10 - 4" ϕ

nutech ENGINEERS

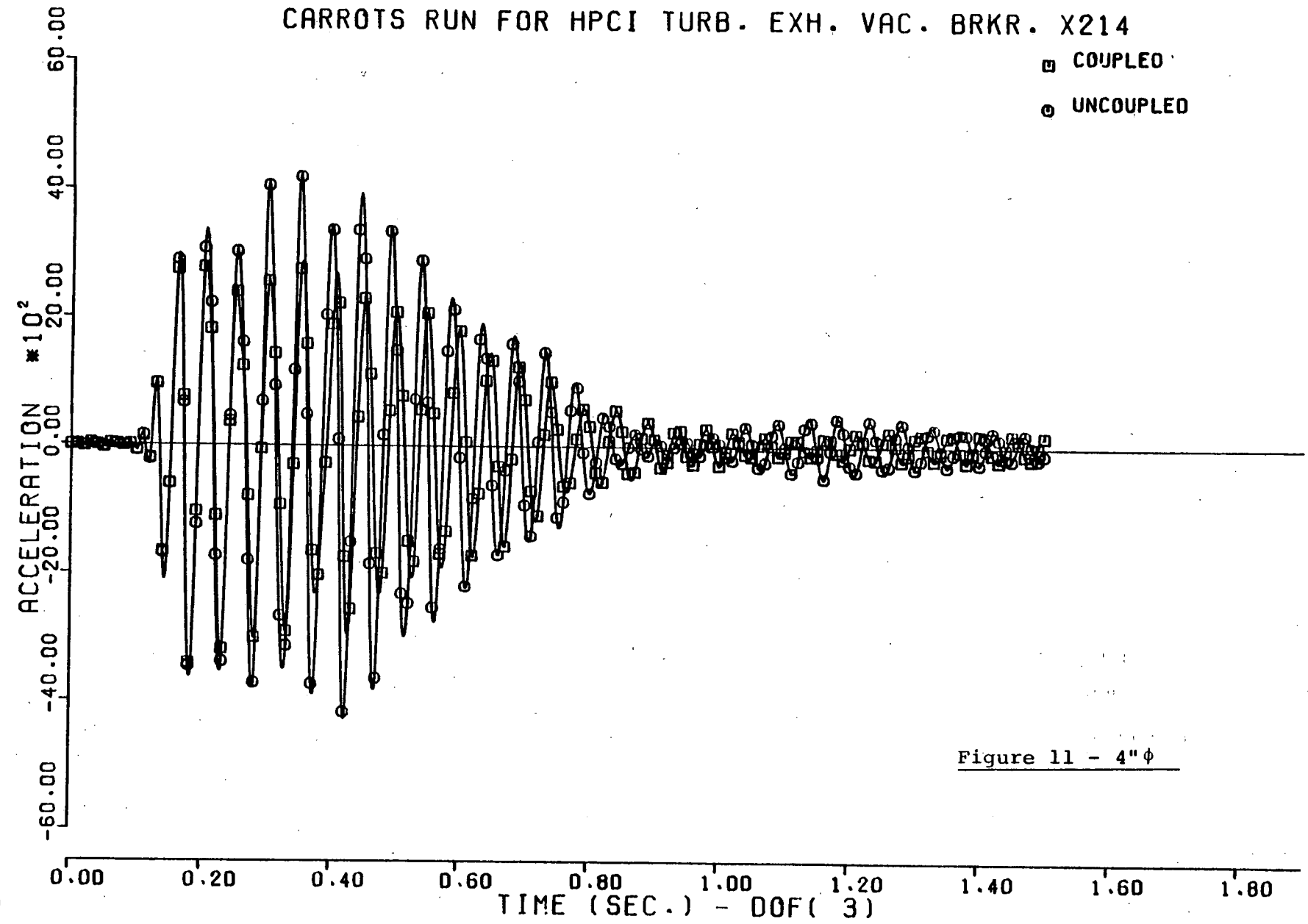

Figure 11 - 4"ϕ

nutech ENGINEERS

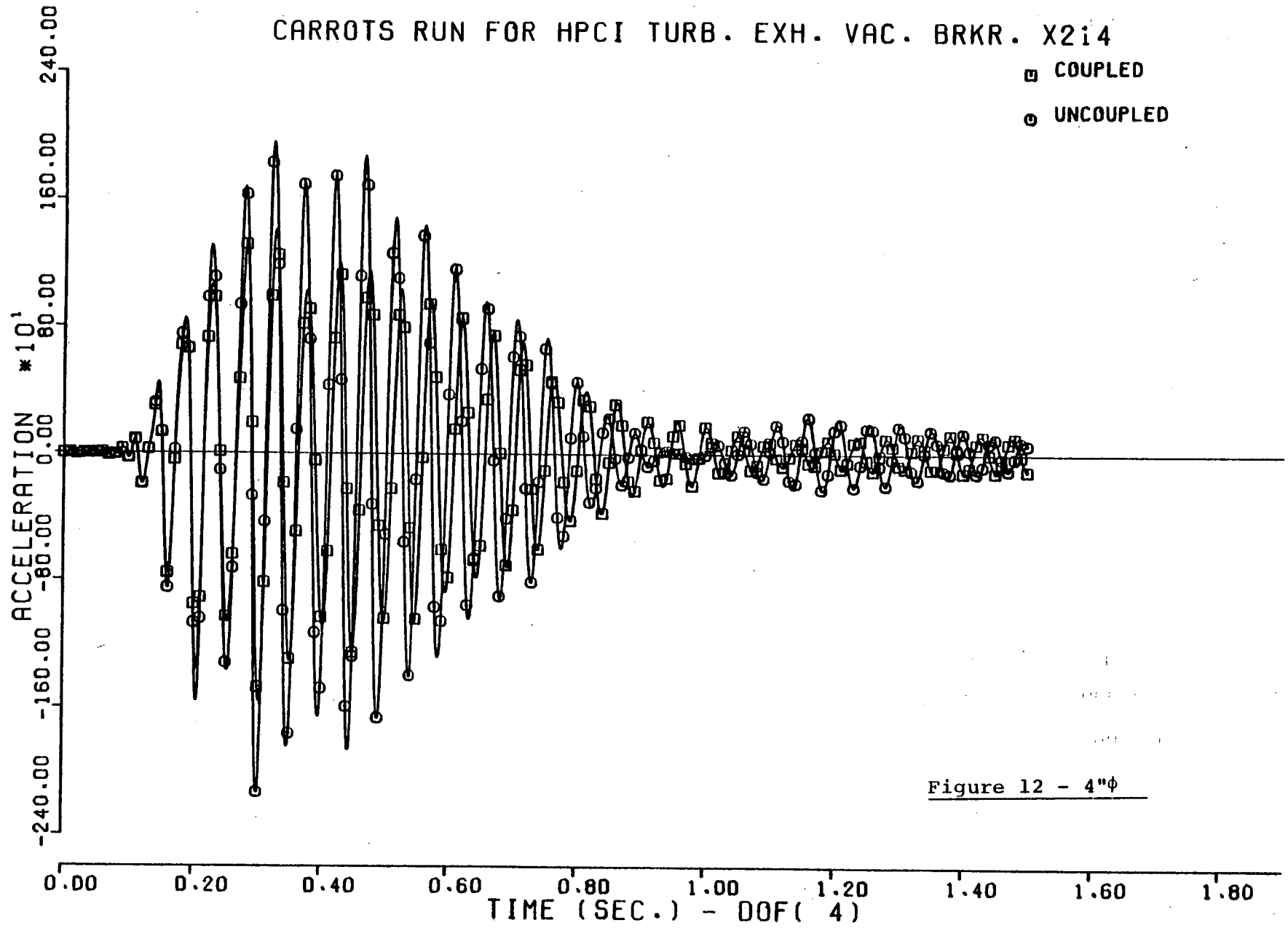

Figure 12 - 4"ϕ

nutech ENGINEERS

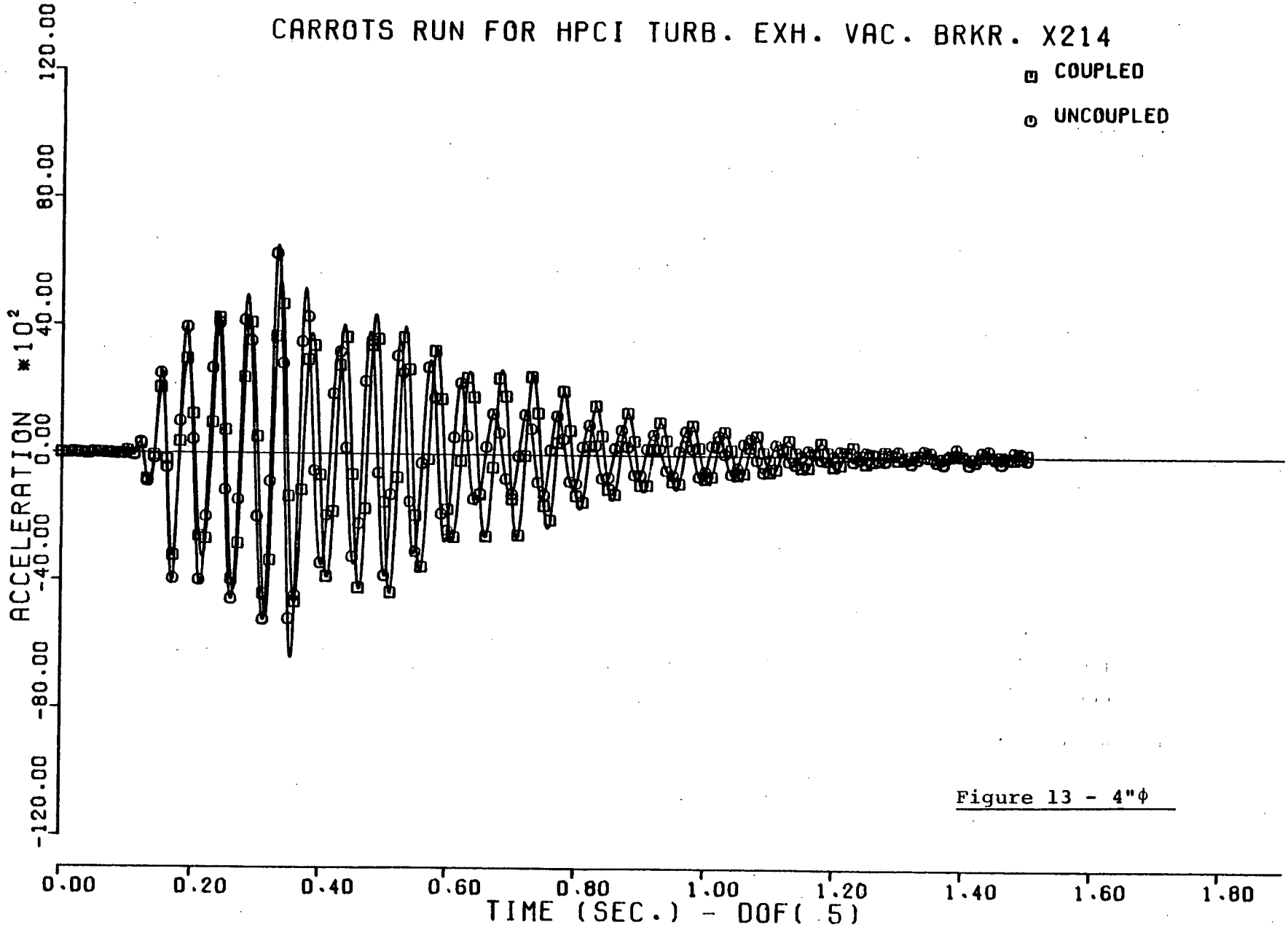

Figure 13 - 4"ϕ

nutech ENGINEERS

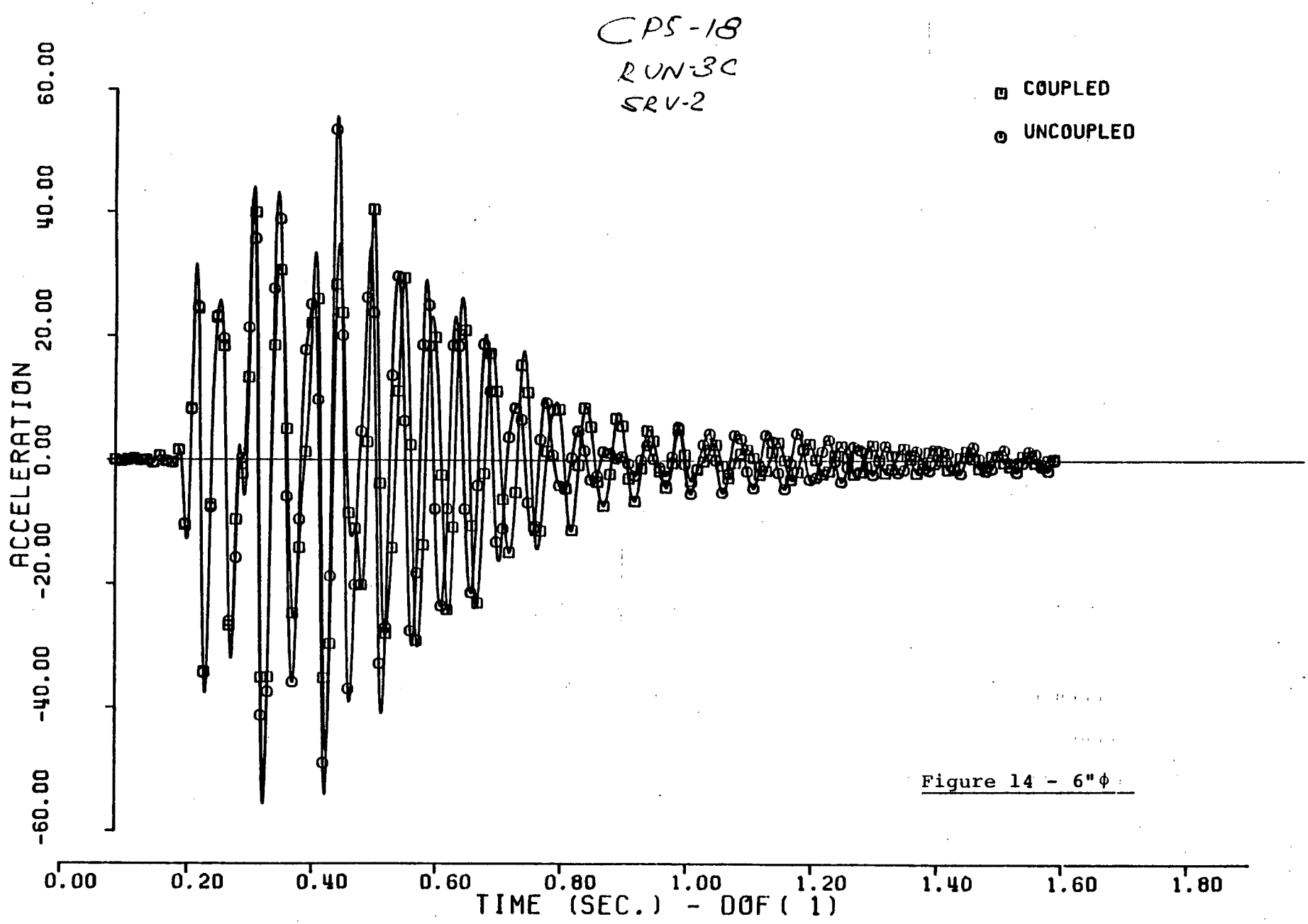

Figure 14 - 6"ϕ

nutech ENGINEERS

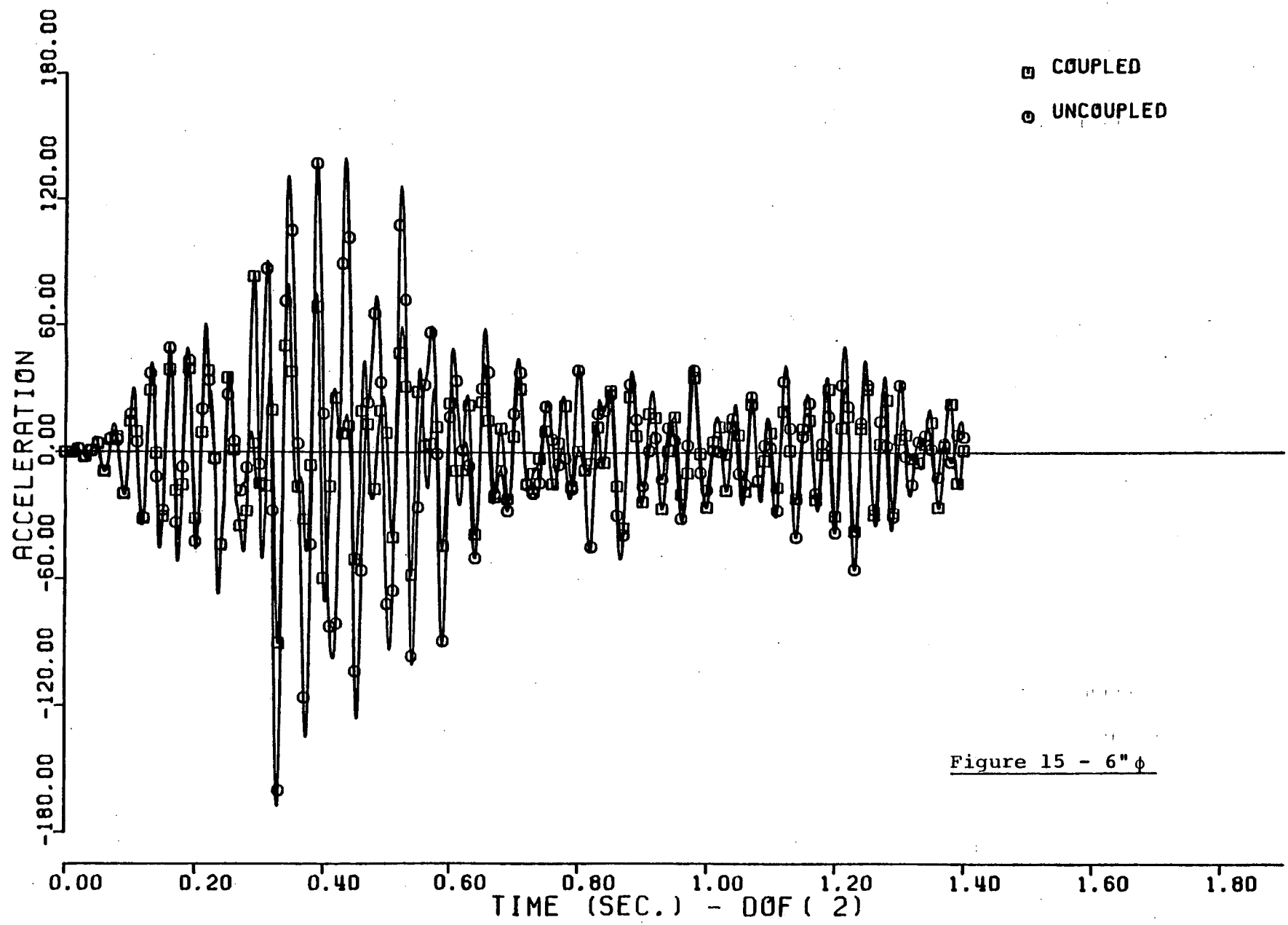

Figure 15 - 6" ϕ

nutech ENGINEERS

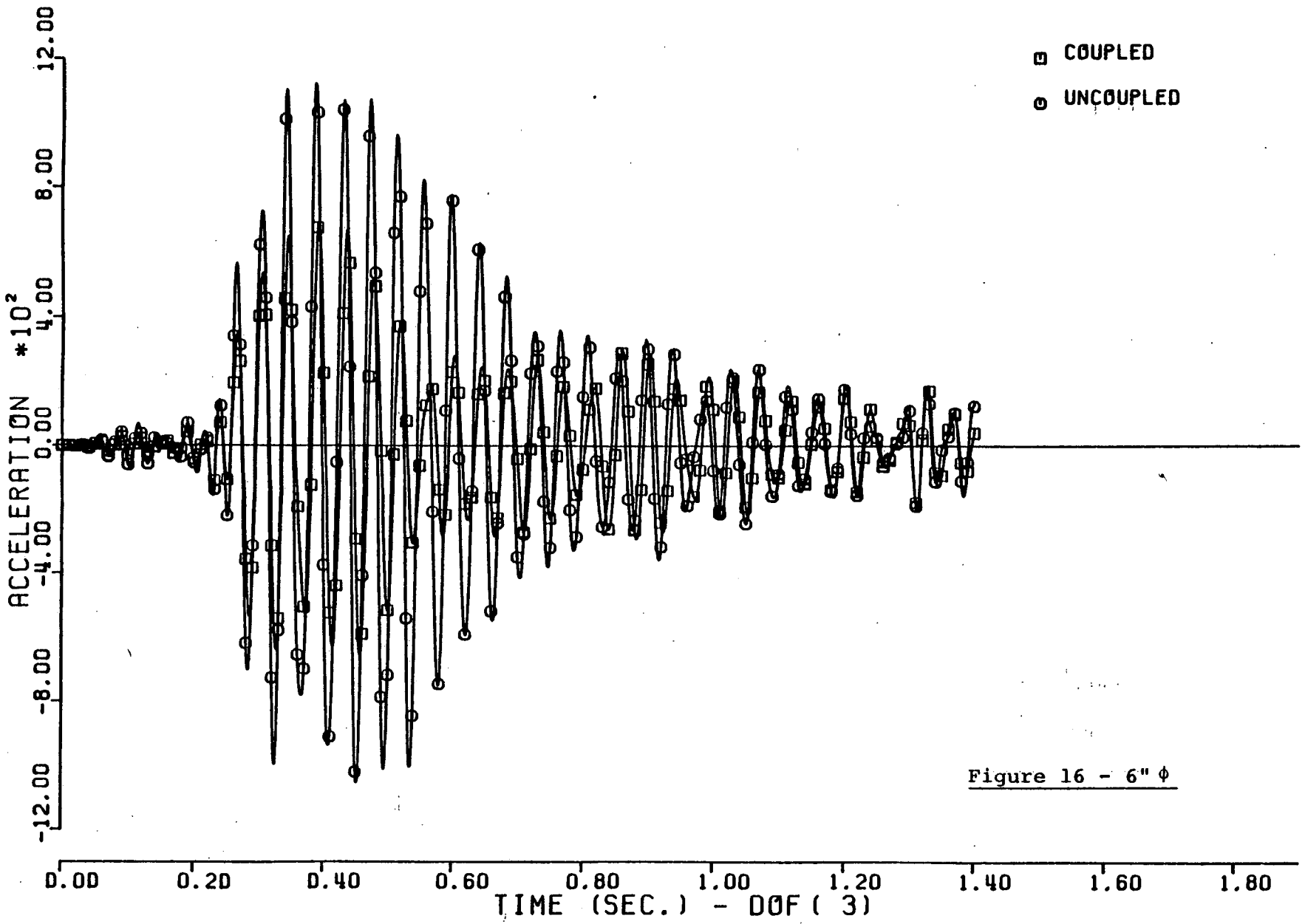

Figure 16 - 6" ϕ

nutech ENGINEERS

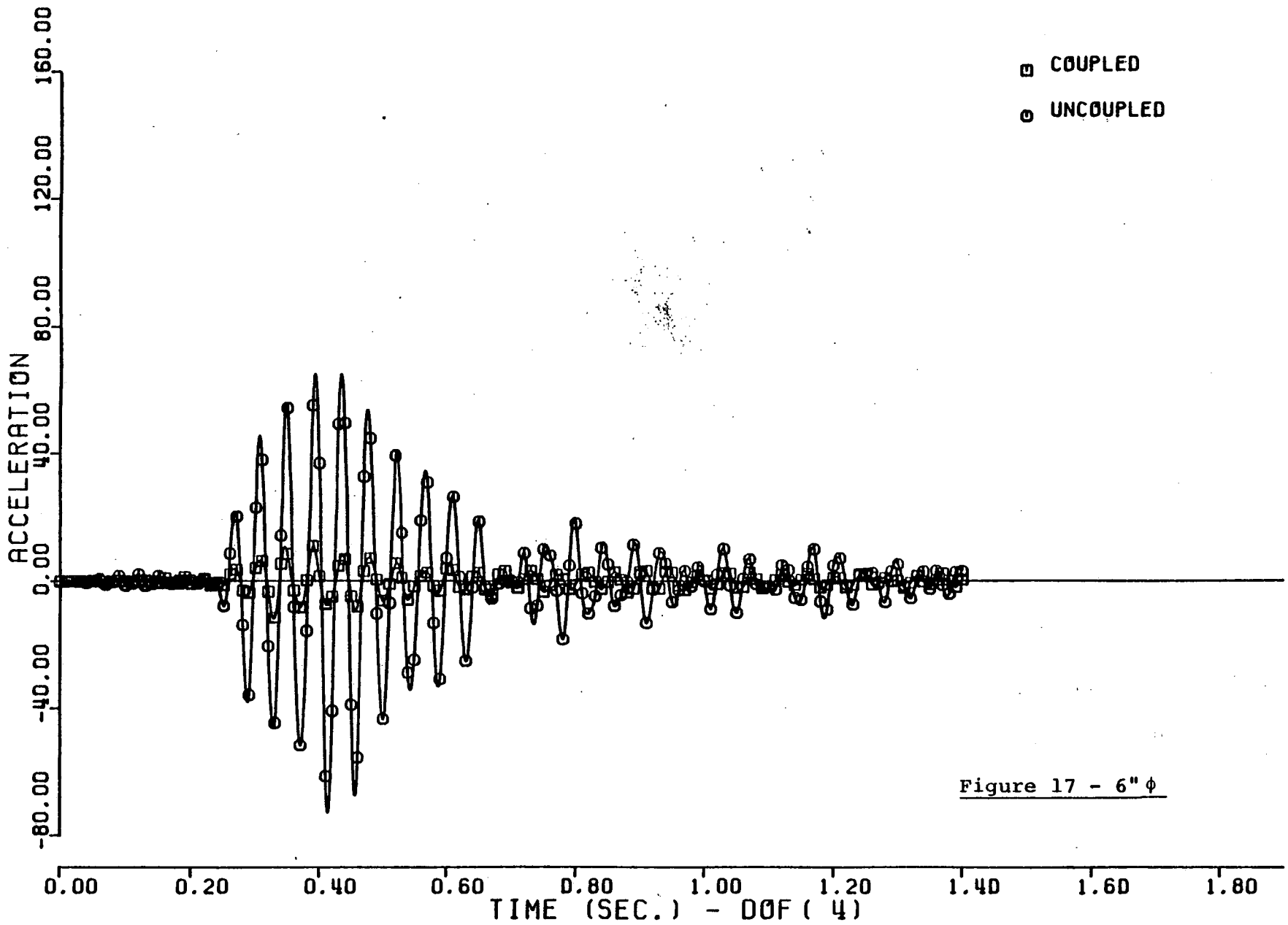

Figure 17 - 6" ϕ

nutech ENGINEERS

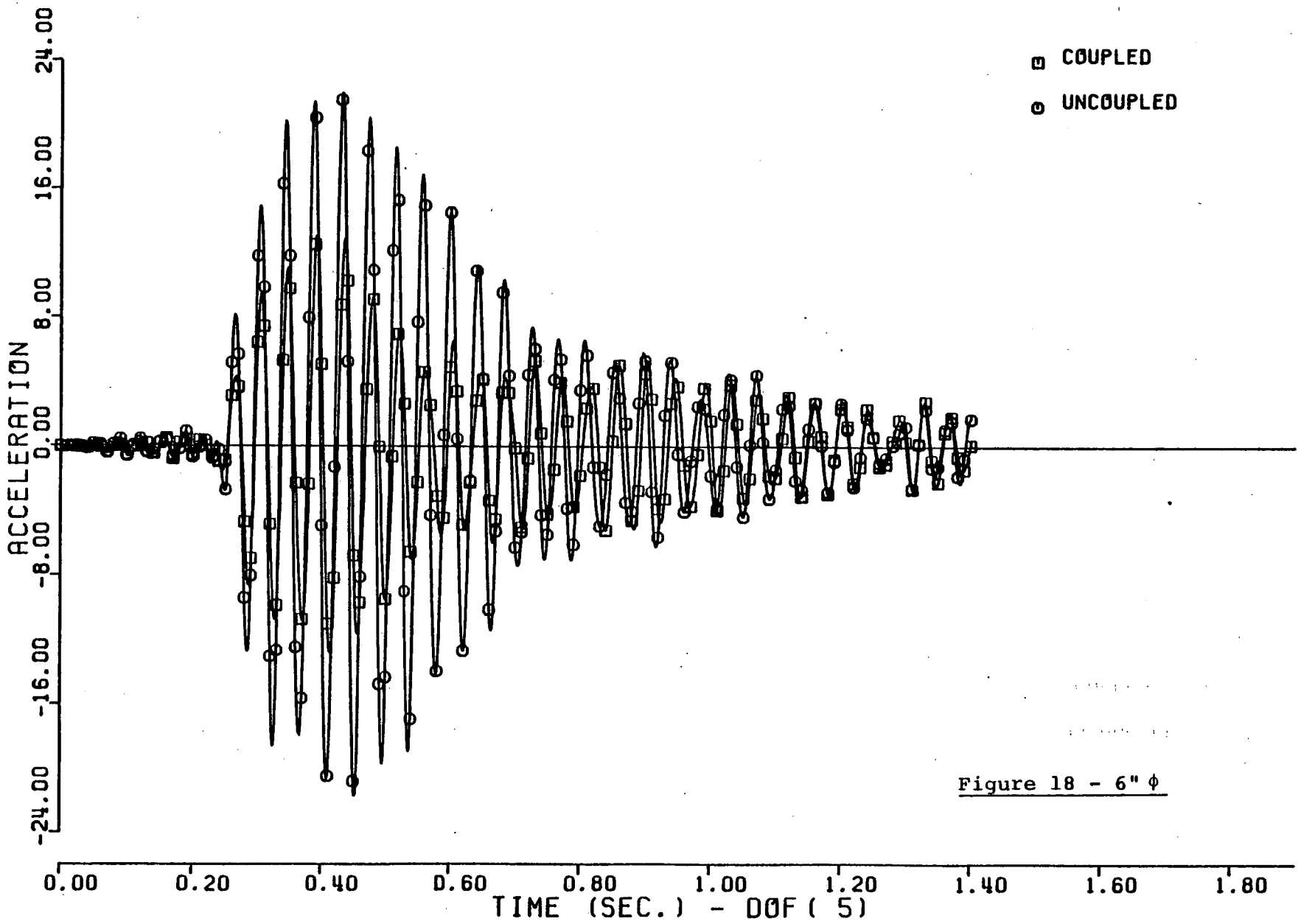

Figure 18 - 6" ϕ

nutech ENGINEERS

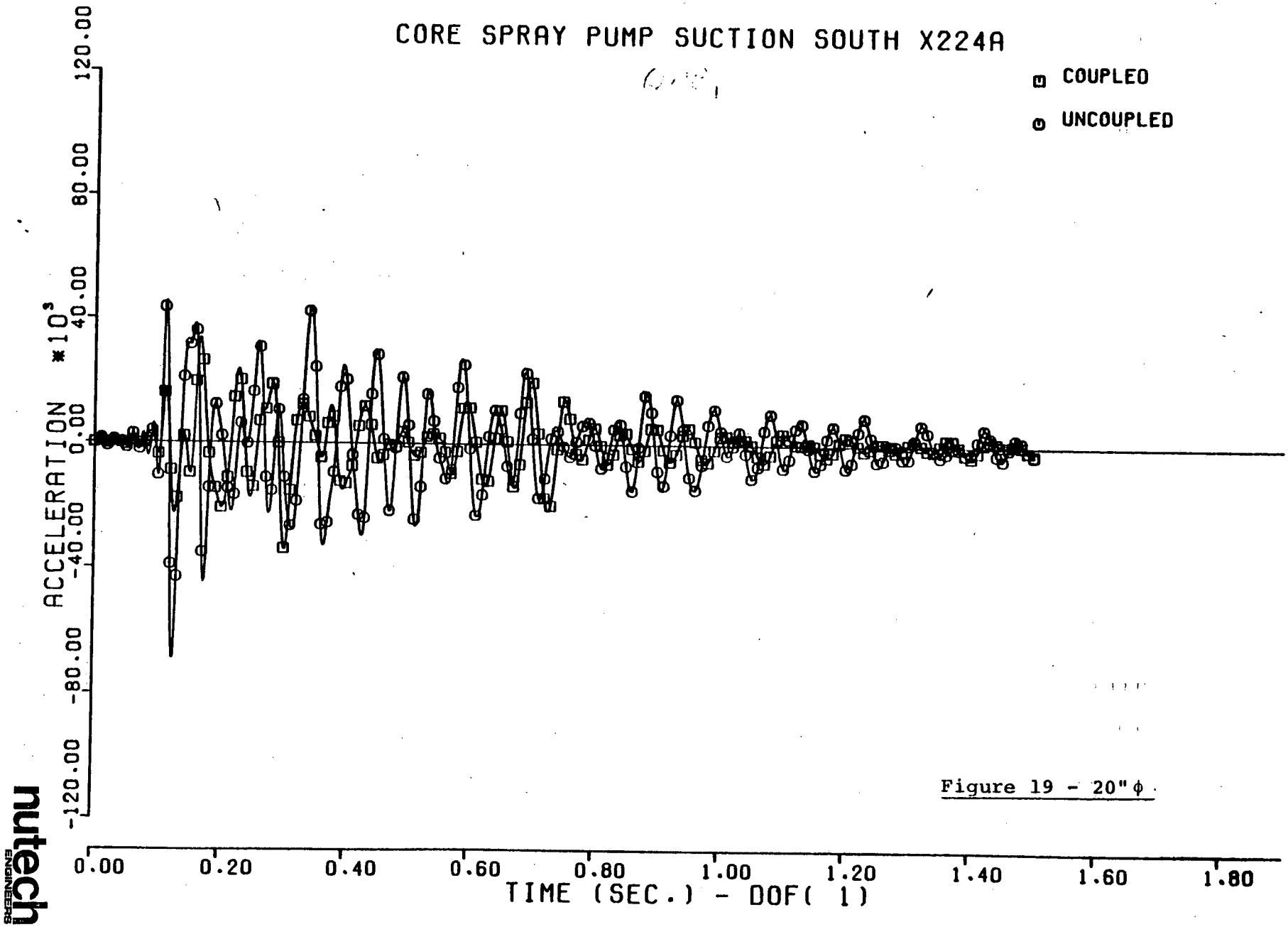

Figure 19 - 20"ϕ

nutech ENGINEERS

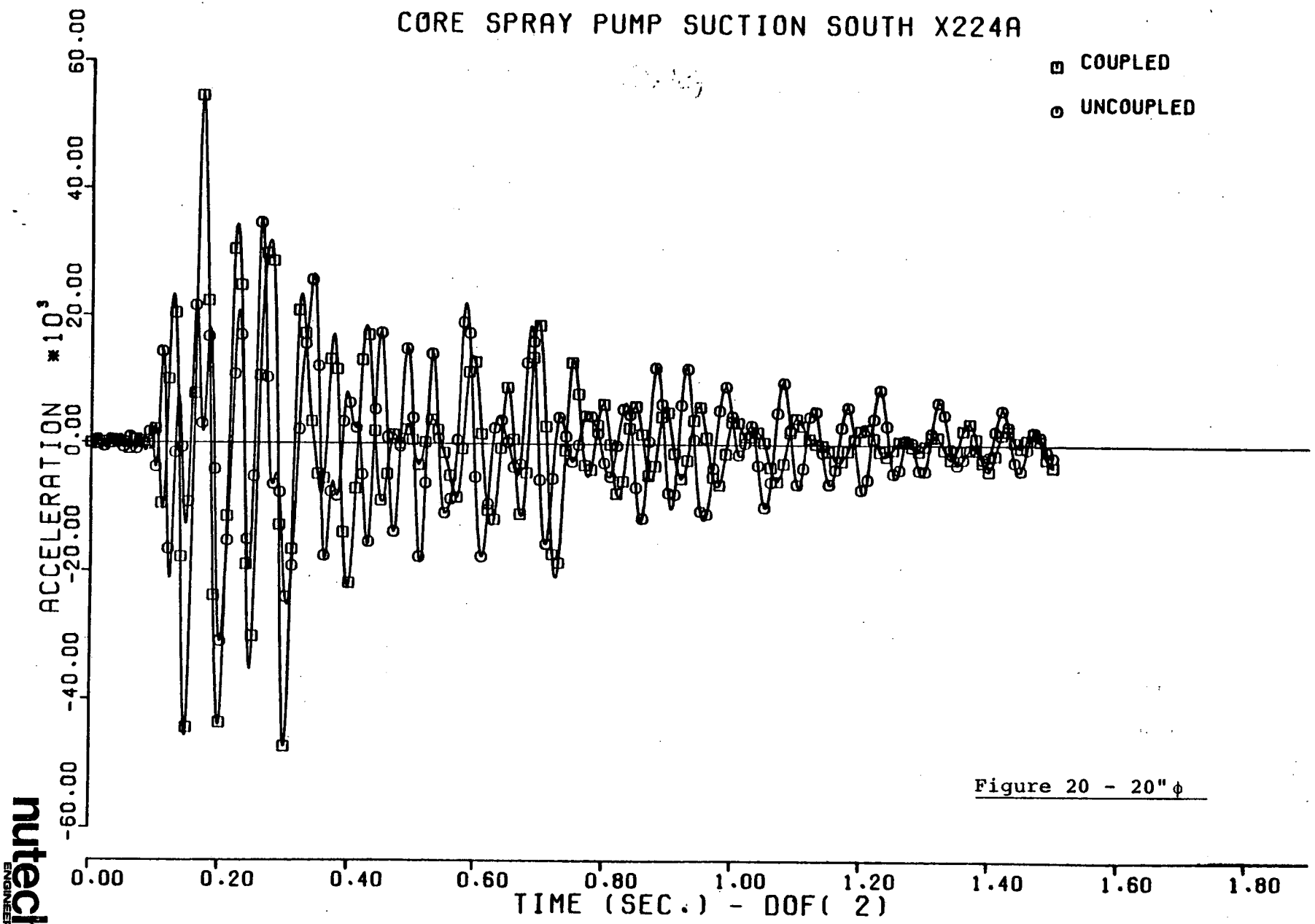

Figure 20 - 20"ϕ

nutech ENGINEERS

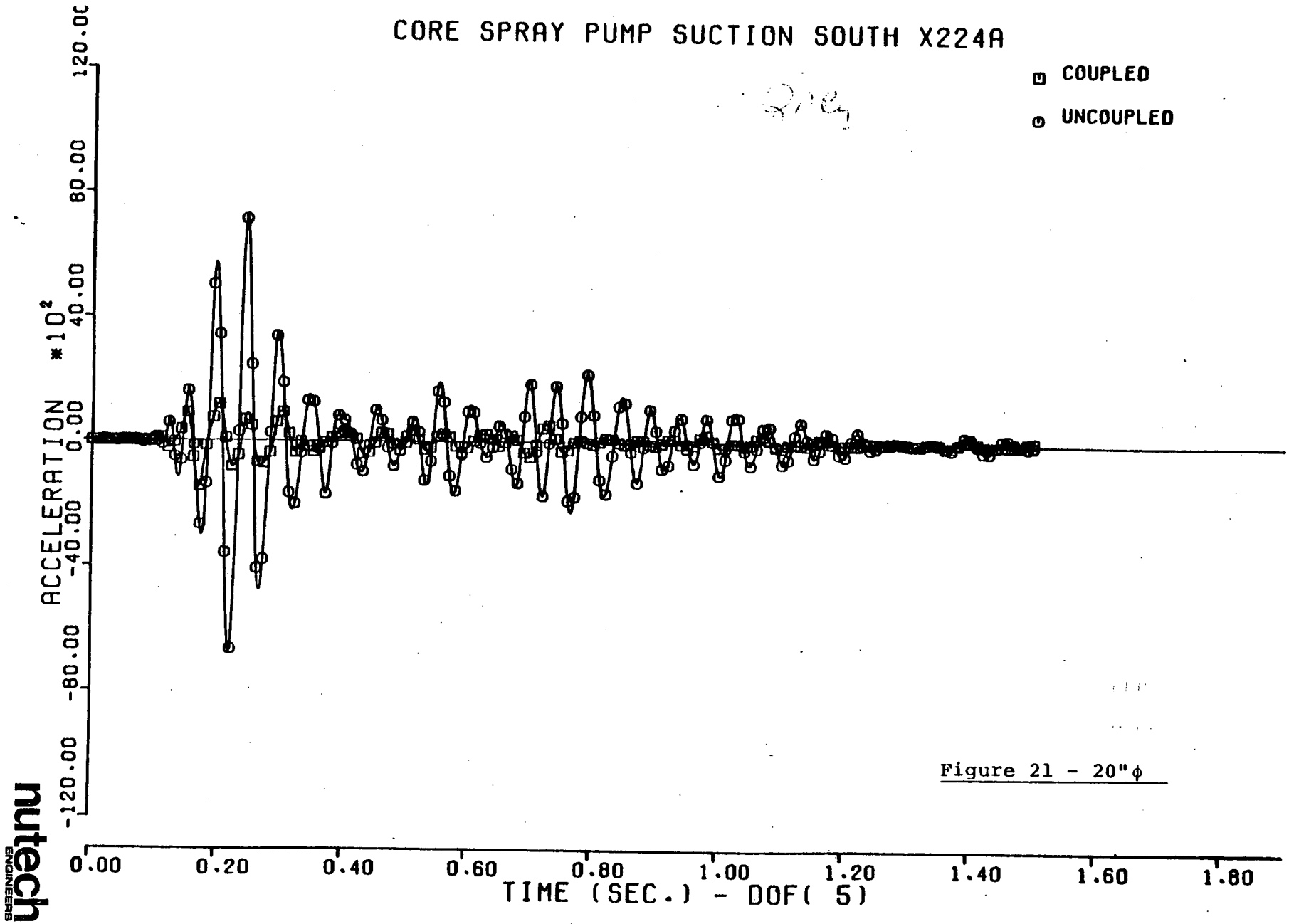

Figure 21 - 20"ϕ

nutech ENGINEERS